DEVELOPMENT OF RADAR ALTIMETRY DATA PROCESSING IN THE OCEANIC COASTAL ZONE

ESA/ESRIN Contract No. 21201/08/I-LG (CCN 3)

Deliverable on

Local Tide Model for the West Iberian Region

Version 1.1

Code	COASTALT-D2.2-1.0	**Edition**	1.1	**Date**	10/10/2010
Client	European Space Agency	**Final User**		-	

	Name	Signature	Date
Written by	UPorto (Machiel Bos and Joana Fernandes)		10/10/2010
Approved by			
Revised by			
Authorised by			

DISSEMINATION	COPIES	MEANS
ESA, Jérôme Benveniste, Salvatore Dinardo and Bruno Lucas	1	Electronic
NOCS, Paolo Cipollini	1	Electronic

SUMMARY OF MODIFICATIONS

Ed.	Date	Chapter	Modification	Author/s
1.1	10/10/2010	Reference Documents	Update of [RD1[	J. Fernandes
1.1	10/10/2010	2.2	Figure 5 has been changed	J. Fernandes
1.1	10/10/2010	2.3	To improve the accuracy of the tide model, the quasi-linearised bottom friction of Le Provost (1973) was implemented. This resulted in a new set of tidal solutions for all 11 main tidal harmonics. We also tried to implement topographic wave friction but this did not seem to improve the accuracy of the tidal solutions. Probably because we are region is too small to see the impact of this phenomenon more clearly. Figures 6 and 7 have been added	M.S. Bos, J. Fernandes
1.1	10/10/2010	3	Figures 8, 10 and 11 (previously 6, 8 and 9) have been adjusted., The caption of Figure 9 (previously 7) has been improved..	M.S. Bos J. Fernandes
1.1	10/10/2010	4	A paragraph has been added at the end of section 4. In addition, five new Figures(12 to 16) showing the difference between the pure tidal solutions and the solutions after assimilation of the observations have	M.S. Bos J. Fernandes

			also been added .	
1.1	10/10/2010	5	We have added Figure 17 which shows that the produced tidal elevations give good results at the Leixões tide gauge and, in Figure 18, we have given an example of a computed tidal elevation map. We have also written a short section about the uncertainty of our results. Our error seems to be around 1 cm and cannot be improved because of lack of observations. Since the non-linear harmonics (such as M4). are smaller than this error bar, they were not included in our computations.	M.S. Bos J. Fernandes
1.1	10/10/2010	Conclusions	The first sentence has been rephrased to include the main information about the model (list of all modelled harmonic components, covered region, spatial and temporal sampling). A sentence was also added referring to the inexistence of bathymetric data from the Hydrographic Institute to try to solve the problem found around Leixões	J. Fernandes
1.1	10/10/2010	Appendix A	New figures with the tidal solutions were made. In addition, Figures for harmonics Mf, Mm and Ssa were also added (Figures 27, 28 and 29)) . Units were also added to the top of all colour scales .	M. S. Bos J. Fernandes
1.1	10/10/2010	Appendix B	The values of the tables were updated using the new tidal solutions.	M.S. Bos

TABLE OF CONTENTS

---+

Reference Documents

[RD1] **COASTALT Technical proposal for extended work (Phase 2)**, DRAFT V. 1.0 November 1, 2009, Document Code COASTALT2-TP-10

Acronyms

TP – TOPEX/Poseidon
J1 – Jason 1
J2 – Jason 2
CPU – Computer Processing Unit
IB – Inverted Barometer
MJD - Modified Julian Date
NCEP - National Centers for Environmental Prediction
PREM – Preliminary Reference Earth Model
RD1 – Reference Document 1
RMS – Root Mean Square
SLA – Sea Level Anomaly
UPorto - University of Porto

Summary

This document presents the Deliverable D2.2 for the COASTALT project, CCN 3, CONTRACT N. 20698/07/I-LG and is delivered for fulfilment of milestone M11.

The present report describes the work that has been done at University of Porto (UPorto) concerning the development of a local tidal model for the West Iberian Region.

1. Introduction

To get accurate satellite altimeter measurements near the coast, an accurate tide model is required to correct these measurements for the tidal effects. For this reason a local tide model of the West Iberian Margin was developed in the scope of COASTALT.

1.1. Short review of previous ocean tide models in the region

One of the first studies of the ocean tides in front of the West Iberian coast has been performed by Fanjul (1997). They used a baroclinic model that was forced at the boundaries and run for several years after which tidal analysis provided the tidal maps. All tidal forcing within the area and any loading plus self attraction effects were ignored. Afterwards, Sauvaget et al. (2000) computed the ocean tides in this area using a barotropic finite element model. However, any loading and self-attraction effects were still ignored. Also the ocean tide model of Fortunato (2002) and Marta-Almeida and Dubert (2006) miss these effects.

The most recent ocean tide model of this region, called IBER01, has been presented by Benavent et al. (2009). They used a barotropic model that was forced by tidal elevations at the boundaries and used an a-priori model for the loading and self-attraction effects. In addition, they assimilated tide gauge data and satellite altimetry into their model using the representer approach of Egbert et al. (1994).

1.2. Global Ocean Tide models

In the last years some new global ocean tide models have been published and we have investigated how they differ from each other in our area of interest. These models are FES2004 (Lyard et al., 2006), EOT08a (Savcenko and Bosch, 2008), GOT4.7 which is an update of GOT99.2b (Ray,1999), TPXO.7.2

(Egbert and Erofeeva, 2002) and an older one called NAO.99b (Matsumoto et al., 2000). For each harmonic we computed the Root Mean Square (RMS) of the vector difference between each model and the mean ocean tide for our area of interest. This mean ocean tide was computed by taking the average of the 5 before mentioned global ocean tide models. By defining the tidal amplitude and phase-lag at each grid point as a vector, the vector difference can be computed. We have also computed the maximum length of this vector difference with the mean tide at each grid point. These results are shown in Figure 1 and 2 for the semi-diurnal and diurnal harmonics respectively.

Figures 1 and 2 clearly show that harmonic M2 has the largest RMS and maximum differences. This is caused by the fact that the tidal amplitude for this harmonic is the largest. Next, these figures show that the largest errors occur near the coast and are of the order of 1-2 cm. Areas with especially large errors are near Vigo, due to its complex coastline with many inlets, and near Gibraltar.

In Figure 2 one can see that for the diurnal harmonics the RMS of the vector differences is below 1 cm.

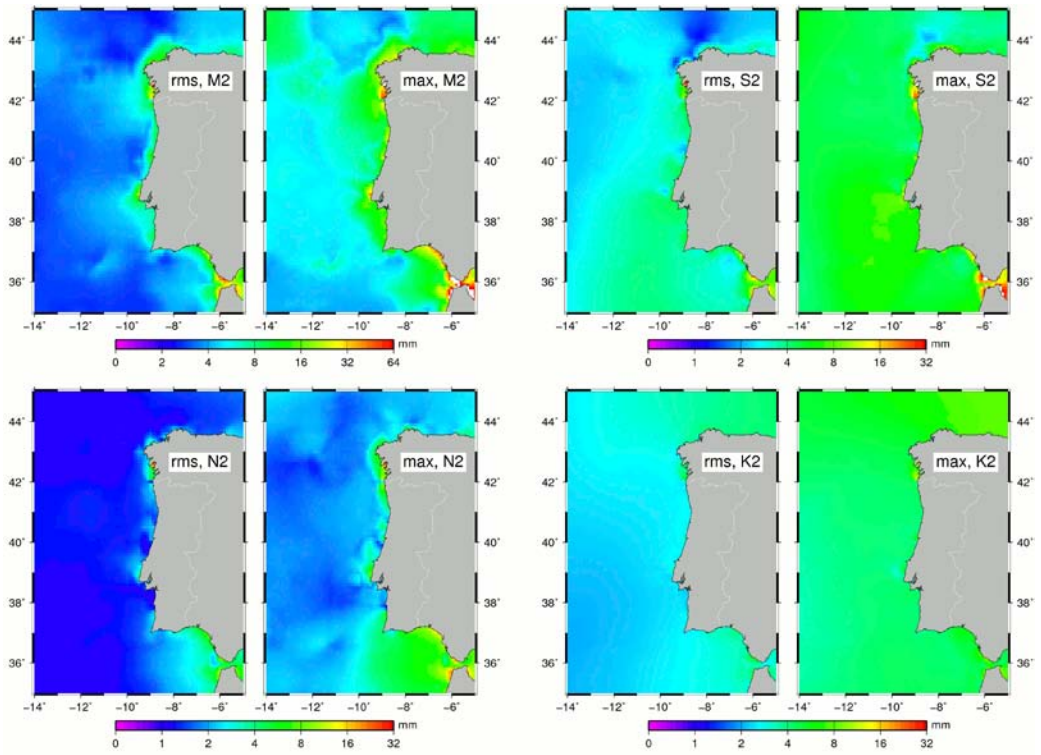

Fig 1. The RMS and maximum differences between the mean field and FES2004, GOT4.7, NAO.99b, TPXO.7.2 and EOT08a respectively, for the four largest semi-diurnal harmonics.

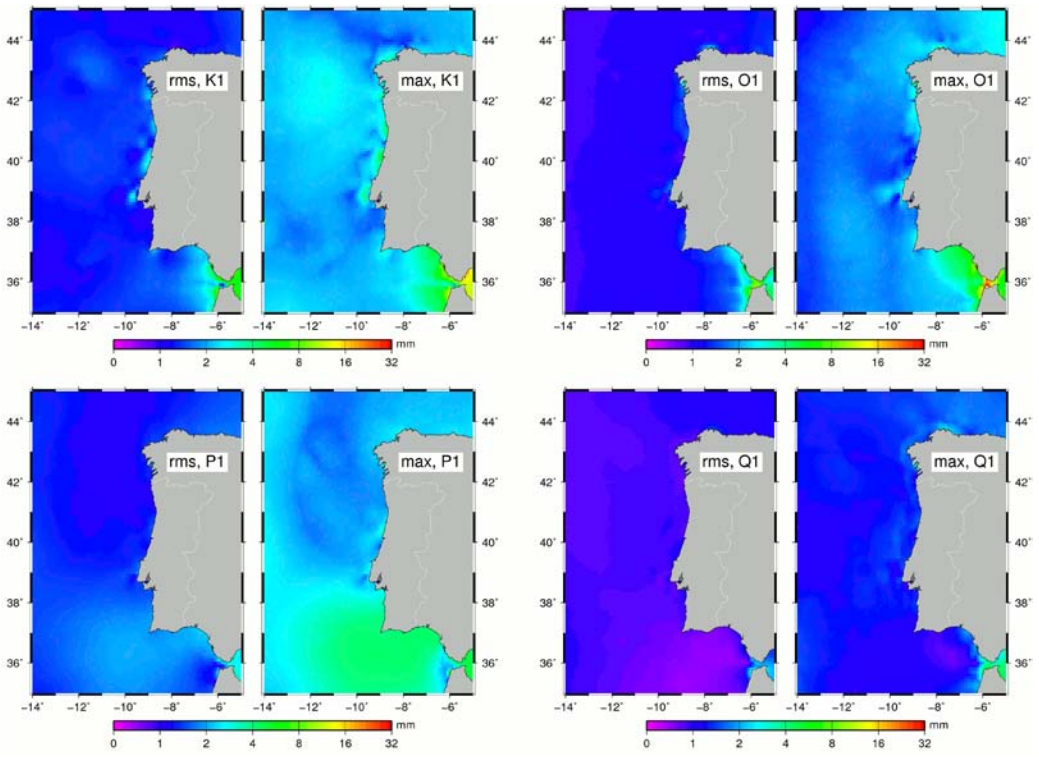

Fig. 2. The same as Figure 1 but for the four largest diurnal harmonics.

2. Model description

Ocean tides are generated by the gravitational attraction of the Moon and Sun. In fact, it is only the horizontal component of these gravitational forces that is important. A very good approximation, which is used in most studies, is to consider that the ocean currents can be assumed to be equal over the whole water column. Thus, we use a barotropic model instead of a baroclinic one. Although the tidal currents are in reality not equal over the whole water column, the computed tidal elevations for a barotropic tide model describe reality very well.

Another assumption is that the advection terms and horizontal eddy viscosity can be neglected. In addition, because the tidal elevation is much smaller than the water depth, we can ignore the influence of the tidal elevation on the total height of the water column. All these assumption together lead to the well known Laplace Tidal Equations.

The Laplace Tidal Equations are differential equations that can be solved by integration over time. However, since the objective was to have a local tide model with a very high spatial resolution of 1 by 1 km, the necessary time step becomes very small and the integration becomes a computational demanding task. Another approach that has been chosen in this research was to solve the differential equations in the frequency domain. Since the tides are periodic, one can divide the forcing in a set of tidal frequencies, normally called harmonics, and solve the differential equations for each harmonic separately. This The

software used in this study was developed by Bos (unpublished) and solves the Laplace Tidal Equations using finite differences. We call the model results WITM (West Iberian Tide Model).

The actual computations have been performed on a cluster. Although only one computing node was used, the fact that we used a relatively high spatial resolution grid made it necessary to have at least 16 Gbyte of memory.

To compute the ocean tides one needs to have a bathymetry which was taken from ETOPO1 (Amante and Eakins, 2009). It has been plotted in Figure 3.

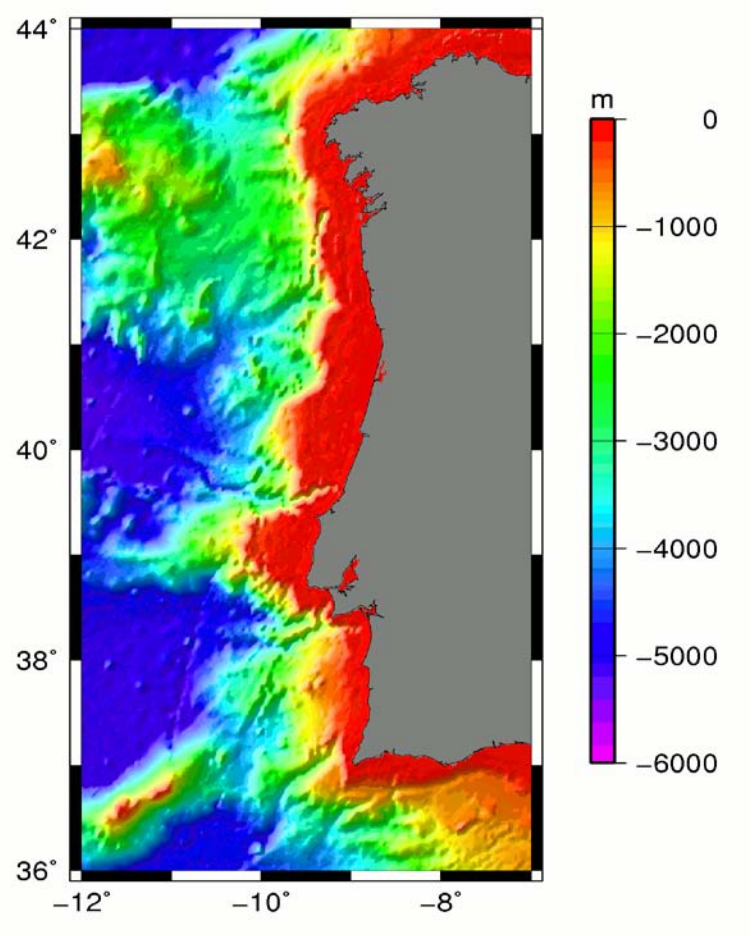

Fig 3. The ETOPO1 Bathymetry

2.1. Open boundary conditions

Since we are computing a local tide model, values at the open boundaries are required. The tidal elevations of the FES2004 model were used for this purpose. To get an idea of the sensitivity of this choice, we have computed the tides for harmonic M2 also using the models GOT4.7, EOT08a and TPXO.7.2 to provide the values at the open boundaries. The results are plotted in Figure 4 and show the RMS and maximum difference with the mean field. One can see that the largest differences occur near the coast and can be as large as 8 mm.

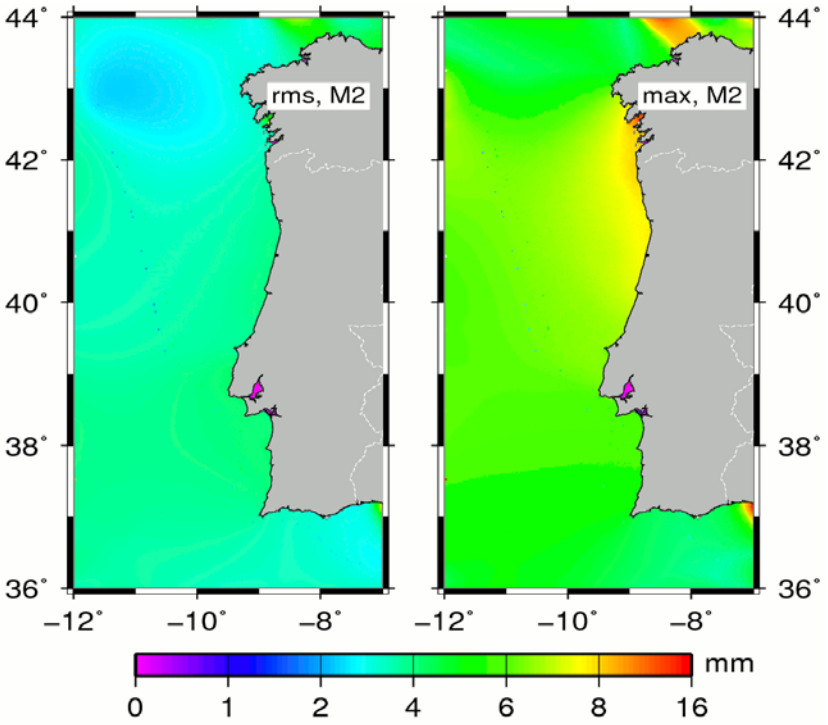

Fig 4. The influence on the tides using different global ocean tide models at the open boundaries for harmonic M2. The left figure shows the RMS. The right figure shows the maximum difference with respect to the mean field.

2.2. Tidal potential and ocean tide loading

Besides the forcing at the open boundaries we applied the tidal potential force inside the domain. The tidal elevations at the open boundary generate the main forces that determine the ocean tides in our area of interest. The effect of including the tidal potential forcing changes the tidal amplitude between 2 and 8 millimetres for harmonic M2 and always improves the fit with the altimetry observations and mostly also the fit with the gauges along the coast.

In addition, we have computed the ocean tide loading inside the domain on a 0.1 by 0.1 degree grid using the GOT4.7 ocean tide model and the Preliminary Reference Earth Model (PREM) for the elastic properties of the Earth. Note that this loading consists out of the self-attraction and deformation of the ocean bottom. For harmonic M2, this loading map is presented in Figure 5. The influence of the ocean tide loading on the results is minimal. For harmonic M2 including ocean tide loading changes the amplitude by around 1 mm in the open ocean and up to 5 mm at the coast. However, including ocean tide loading does not always improve the fit with the tide gauges. For harmonic O1 the effect of ocean tide loading is not noticeable in the open ocean and only 1 mm at some tide gauges.

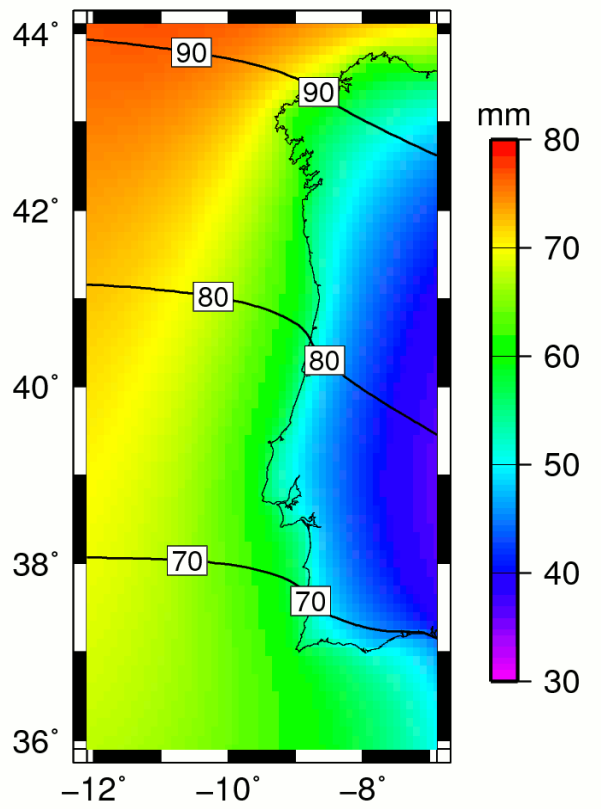

Fig 5. The self-attraction and loading deformation for M2.

2.3. Bottom friction

Ocean tide models are normally very sensitive to the modelling of the bottom friction. For this reason much has been written on this topic. In the deep ocean the bottom friction has a smaller impact on the results and one can normally use a linear bottom friction law. Thus, the amount of bottom friction scales with the tidal current.

A linear bottom friction model allows the computation of the tidal maps for each harmonic separately. However, it is well known that a quadratic bottom friction model, which is thus non-linear, describes reality better. An interesting review of this is given by Lee et al. (2001). Since the tidal currents are mostly larger in shallow water, Egbert et al. (1994) scale their coefficient of the linear bottom friction inversely with the depth to try to take this into account. This approach has been copied.

However, this still does not take any non-linear interaction between the different harmonics into account. It could well be that the bottom friction for our smaller diurnal tides is influenced by the currents of the dominant M2 tide. To investigate this possibility, we have implemented the quasi-linearised bottom friction scheme of Le Provost (1973). This scheme has been used in FES2004 (Lyard et al., 2006) and has proven to give good results.

For the semi-diurnal tides both the linear and the quasi-linearised bottom friction model gave both excellent results. However, for the diurnal tides the linear

friction model did not dissipate enough and required an increase of the friction coefficient. The quasi-linearised bottom friction model behaved better and has been used to compute the final results.

For realistic values of the bottom friction coefficient (also known as Chezy coefficient) of around 0.003, one could not see much dissipation due to bottom friction at any tidal harmonic. Thus, non-linear interaction does not alter our earlier conclusion that the bottom friction effect is small.

Another source of tidal dissipation is topographic wave drag which causes internal tides over steep topography. From the figures given by Jayne & Laurent (2001) and Lyard et al. (2006), one can see that the tidal dissipation due to topographic wave drag is larger for the West Iberian coastal shelf edge than due to bottom friction.

Therefore, we have implemented this topographic wave drag into our numerical model using a simplified version of the approach of Jayne & Laurent. Our wave drag model is of the form:

$$\tau = C_d N h^2 \qquad (1)$$

Here N is the buoyancy frequency, h^2 the roughness and C_d a scaling factor. The buoyancy frequency, also called the Brünt-Vassala frequency, has been modelled as a constant between a depth of 0 and 500 metres, after which it decreases linearly to zero at 8000 metres depth, see Figure 6. The buoyancy frequency depends on the stratification of the ocean and can be computed using a more refined manner, but considering the simplification already implied by using Eq. 1, this simple model was assumed to be sufficient.

The roughness was computed using ETOPO1 by computing the variance of the bathymetry along East-West and North-South lines. Thus, we computed two roughness fields, one for each direction. As a result, we have different wave drag models for the two directions. By using a moving window of around 0.1 degree to compute this variance, the roughness factor changes from place to place. The normalized roughness fields h^2 (no unit) are plotted in Figure 7.

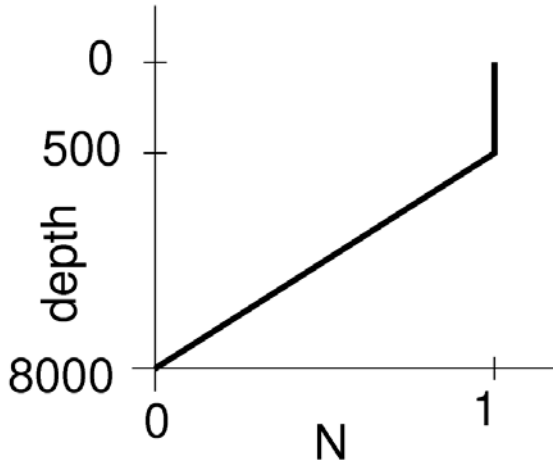

1.

Fig. 6 The parameterization of the normalized buoyancy frequency.

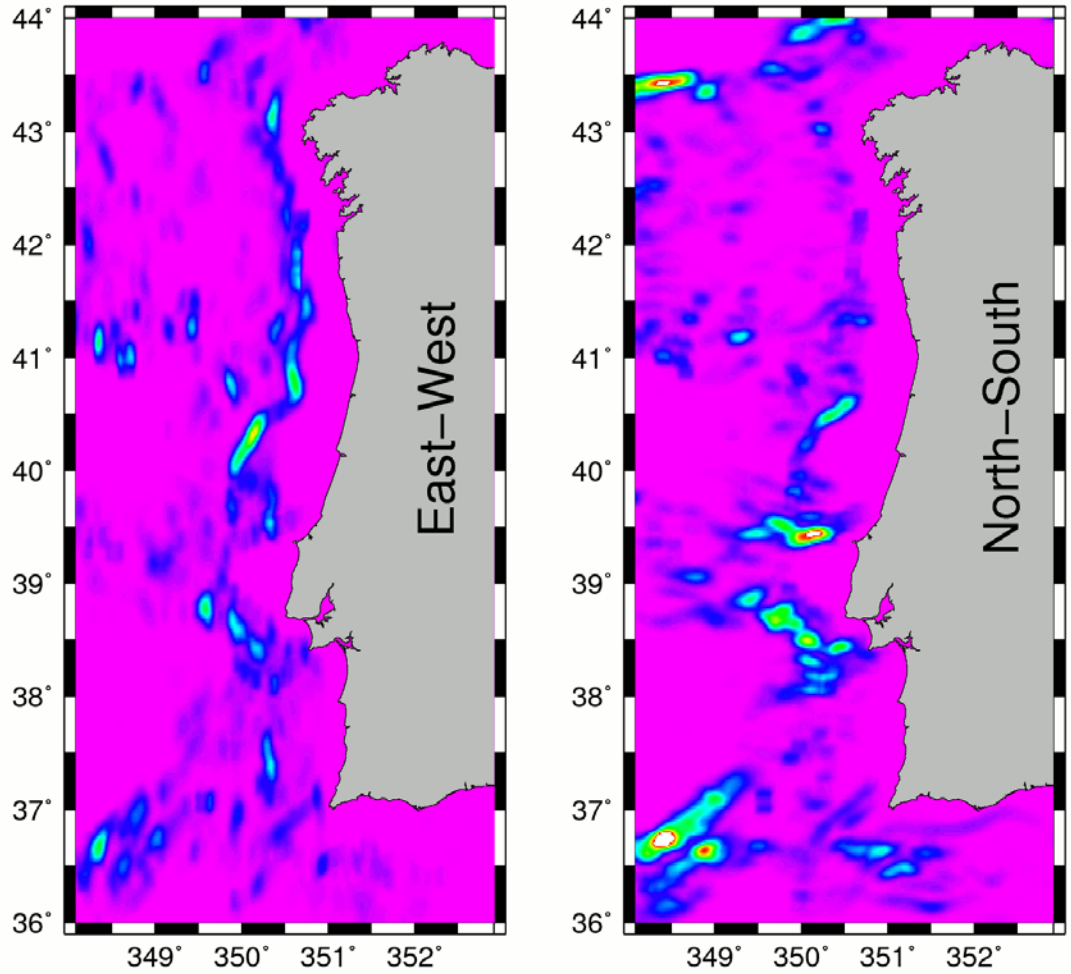

Fig. 7. The normalized roughness h^2 for the East-West and North-South direction. A linear rainbow colour scale is used where purple is zero and red is 1.

However, adding topographic wave drag gave strange results in the deep ocean which seems to imply that our modelling of the buoyancy frequency is too simplistic. Furthermore, this type of friction did not improve our fit with the tide gauge and satellite altimetry observations and has been dropped. It is thought that the area is too small to see a noticeable effect of topographic wave drag.

3. Validation of the ocean tide model with observations

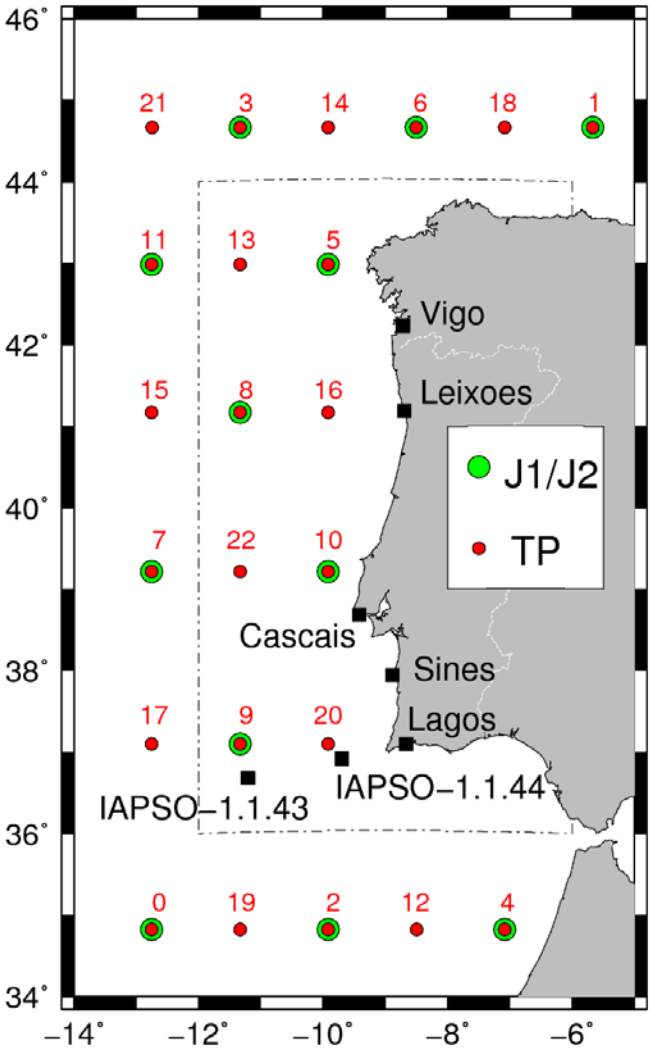

Fig 8. The location of the cross-over points for TOPEX/Poseison, Jason 1 & 2. The red numbers indicate the name of the cross-over point for the TP satellite. Also plotted are the tide gauges used in this study.

An important aspect of any computation of a tide model is its validation with in-situ observations. For this task we have used tide gauge data available in our area, which are few, and cross-over points of satellite altimetry data. The locations of these points (6 tide gauges) are given in Figure 8. Note that we have given each cross-over point of the TP satellite a number in Figure 8 to facilitate the description of our results.

3.1. Tide gauges

The tidal amplitude and phase-lag data of two bottom pressure tide gauge data were taken from the IAPSO dataset (Smithson, 1992). The other tidal amplitude and phase-lag data for the main harmonics at the coastal tide gauges were taken from Fanjul (1997) and Fortunato (2002). For harmonic M2, the comparison with global tide models and the new local tide model WITM are given in Appendix B.

We found that the values at IAPSO-1.1.43 are suspiciously large as are the values at IAPSO-1.1.44. The reason for this is not known. It must be noted that none of the global ocean tide models have assimilated these two values into their model.

The values given for our new model called WITM are good if one takes into account that no assimilation has yet been performed. The most problematic point is Leixões. Varying the bottom friction and using other ocean tide models at the open boundaries did not significantly reduce the misfit. Two possible explanations for this misfit are errors in the bathymetry and some local influence of the river Douro on the tides observed in the harbour.

The Leixões data have been assimilated into the IBER01 model which explains the extremely good fit for this particular model at this location.

3.2. Satellite altimetry

Data are AVISO mono-mission Sea-Level Anomaly (SLA), downloaded in July 2010 after a recent upgrade. SLA data at the crossover locations were generated, for each mission. No crossover adjustment has been performed. In addition, a “Distance to land” field was added. For each mission and cycle the crossover position (latitude, Longitude) were determined. Then, for each pass, the corresponding measurement time Modified Julian Date (MJD), SLA have been interpolated using linear interpolation. According to AVISO, these SLA values have been corrected for ocean tides and ocean tide loading using the GOT4.7 global tide model. If this model were perfect, these data would not contain any residual tidal signal. However, our tidal analysis show some remaining tide signal which will be used to improve our local tide model. The SLA values have also already been corrected for the inverted barometer (IB) effect. We tried to find some residual IB signal in the SLA data using 30 days averages NCEP surface pressure data but this did not reduce the variance of the SLA values.

We removed outliers by simply eliminating SLA values larger than 0.25 m. This happened only once for the Envisat data used in this study and twice for TOPEX/Poseidon. The Envisat has a nearly sun-synchronous orbit which causes problems to observe the S1, S2 harmonics. In fact, all tidal periods near 24 hours such as K1 and P1 are difficult to estimate. Therefore, only the following harmonics were estimated: Sa, Ssa Mf, Q1 , O1 , OO1 , 2N2 , N2, and M2 . The yearly and half-yearly harmonics were included to remove the seasonal signal present in the SLA data. These are caused by non-tidal processes but need to be estimated to improve the accuracy of the tidal analysis (reduce the variance of the residuals). The data analysis was

performed with the program called *versatile_tidana* of Foreman et al. (2009). This program allows unequally spaced data and provides information about the correlation between the estimated tidal parameters. This last item helped us to ensure that the set of tidal parameters estimated for the Envisat data are really meaningful and not significantly influenced by the yearly and half-yearly periods. The best results are obtained for the Jason 1 data. The data span is 7 years and the accuracy of the estimated tidal amplitude at the main harmonics lies normally around the 2 to 3 mm. Similar results are obtained for the TOPEX/Poseidon (TP) phase A, before its orbit change in 2002. This provides a dataset of around 10 years or around 550 observations at the crossover points. Three years of TP phase B data are available after the orbit change. For the first period, the accuracy of the estimated tidal amplitude at the main harmonics is around 3 mm, for the second period this value lies around 5 mm which is also the accuracy for the Jason 2 data.

The accuracy of the estimated tidal parameters using the Envisat data lies around 6 mm.

An example of a time-series at a cross-over point, our number 0 in Figure 8, for the TP satellite, is presented in Figure 9.

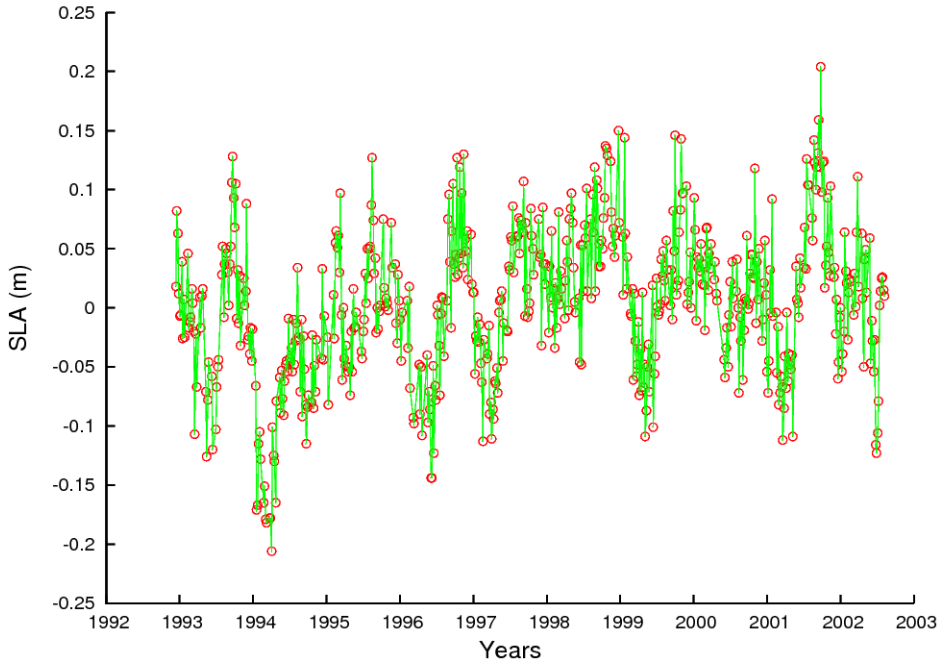

Fig 9. Example of the SLA time-series for the TP satellite at cross-over point 0. The red dots are the SLA observations which are connected with a green line to see their behaviour over time more clearly.

The results of the tidal analyses are plotted in Figure 10 for the TP, Jason 1 & 2 and the Envisat satellite for harmonic M2. The arrow length indicates the observed tidal amplitude. The angle with the positive x-axis indicates the observed phase-lag. The error circle indicates the 95% confidence region.

The fact that the results for the TP, Jason 1 & 2 satellites look very similar seems to suggest that we are perhaps overestimating the error bar.

The results for the Envisat satellite are very noisy and have not been used in this study.

Figure 11 shows the same as Figure 10 but now for the harmonics M2, S2, K1 and O1 and only for the TP satellite. One can see that for the other harmonics the error bar is normally larger than the observed tidal residuals. Thus, assimilating the diurnal harmonics derived from altimetry data into the model seems dubious because one could be assimilating noise into the model instead of making the model more realistic.

After the tidal analysis of the residual satellite altimetry time-series, the values of the GOT4.7 model were added back to the results to get the total observed tide values at the cross-over points.

The tidal analysis results are for harmonic M2 and for the TP satellite given in Appendix B. These results show that our new model performs well in the open ocean.

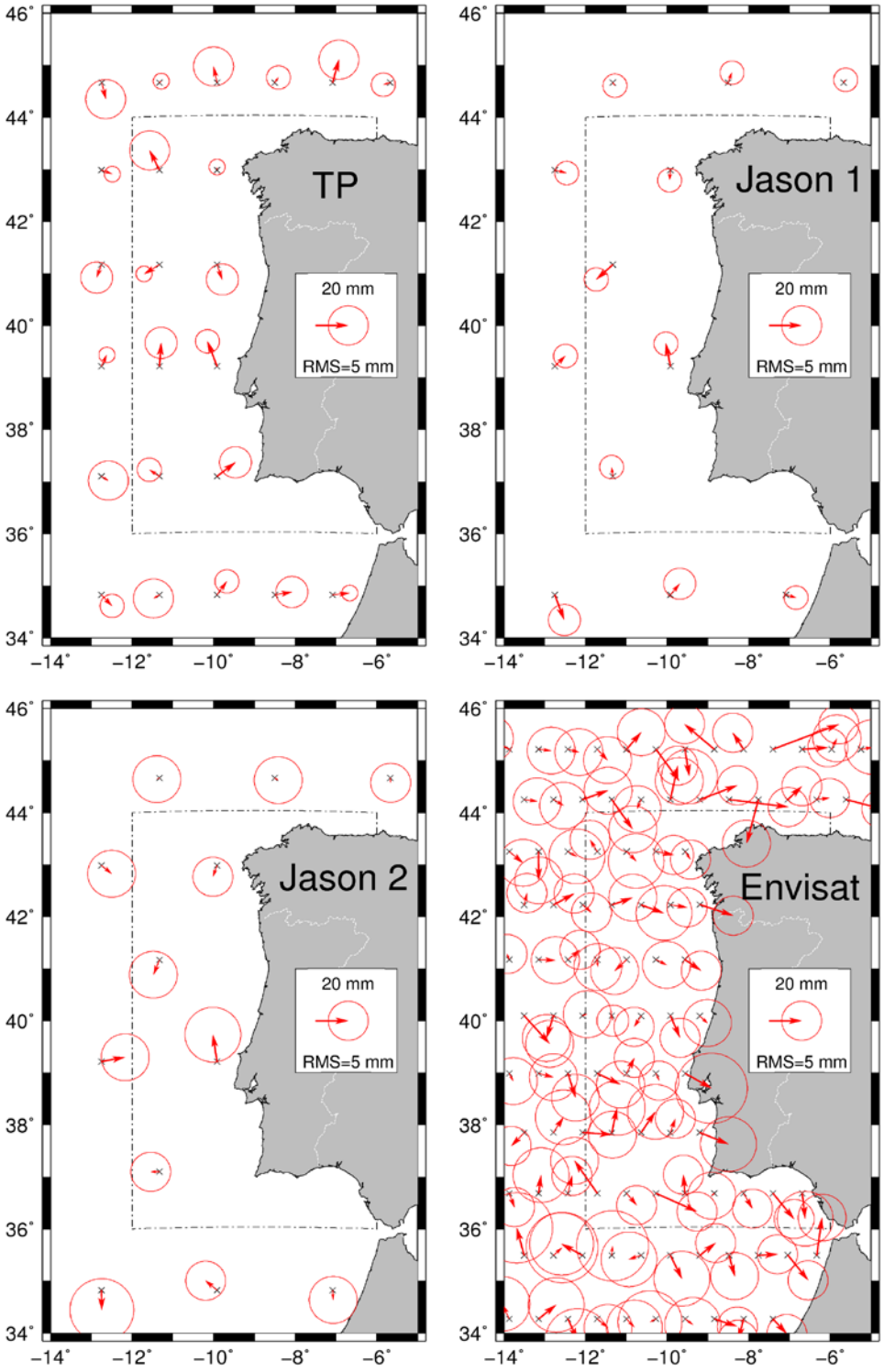

Fig. 10. The results of the residual tidal analysis for harmonic M2 at the cross-over points for the TOPEX/Poseidon, Jason 1 & 2 and Envisat satellite. The arrow length indicates the observed tidal amplitude. The angle with the positive x-axis indicates the observed phase-lag. The error circle indicates the 95% confidence region. The legend shows an observed tide with an amplitude of 20 mm, a zero phase-lag and the 95% confidence region for the case the RMS=5 mm.

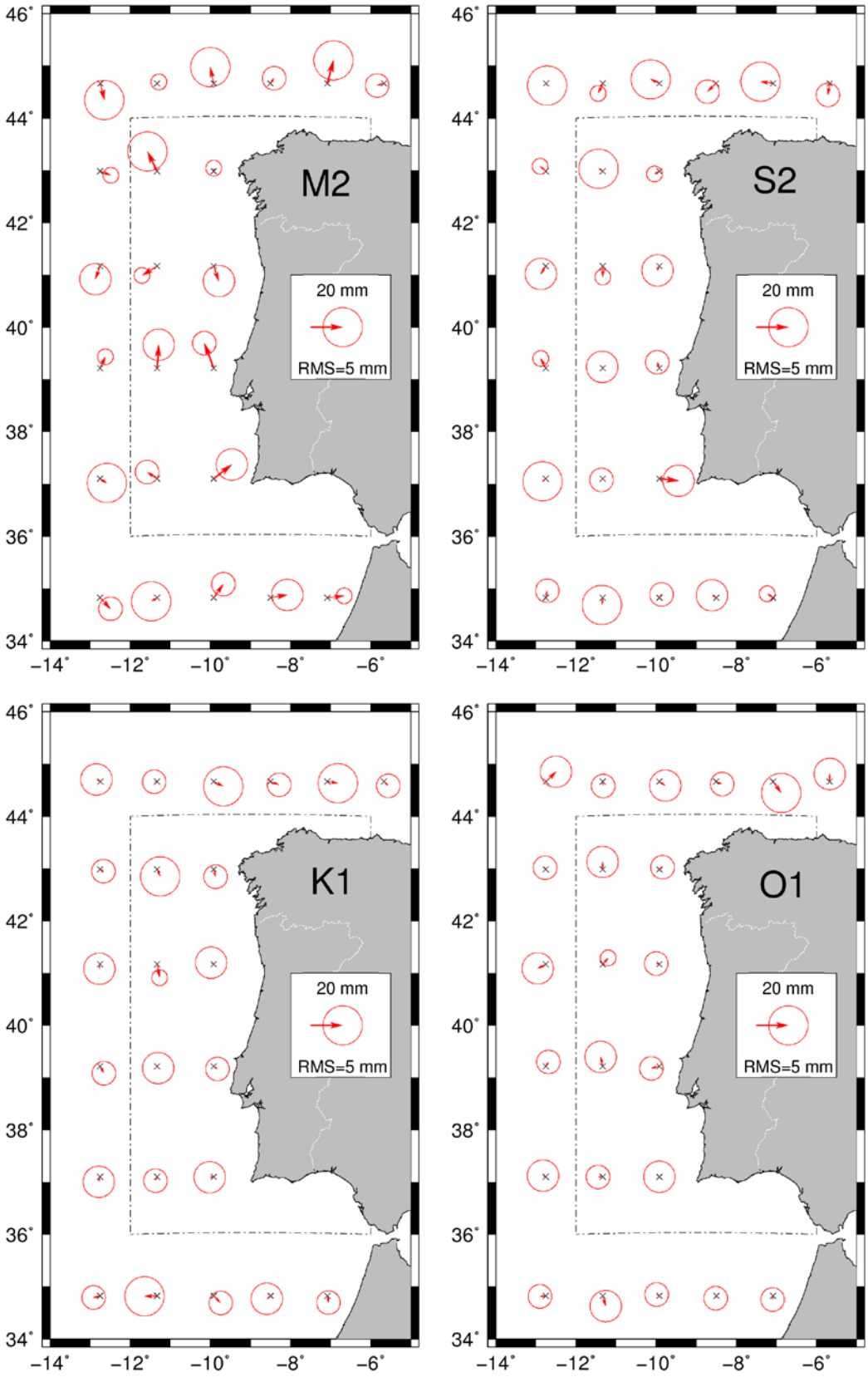

Fig. 11. The same as Fig 10. but only for the TOPEX/Poseidon satellite and for harmonics M2, S2,

4. Tidal assimilation

The comparison of satellite altimetry data and tide gauge data with our new local tide model results show good results but there are sometimes still misfits at the order of 1 cm at some locations. At the coast the fit is sometimes even worse. To provide the COASTALT project with the best possible tide model, we adjusted our local tide model to fit the TP cross-over observations perfectly. The adjustment was made by fitting Gaussian bell-curves to the residual altimetry observations using least-squares. The Leixões gauge observations were not included in this process because of the suspicion that this gauge is not really representative of the tides in the region. The other tide gauges were assimilated into the model. The result is a local tide model with high spatial resolution but smoothly adjusted to get perfect fit with the observations.

The adjustments were computed, for each harmonic, for the in and out-phase (also called quadrature) of the tide. For harmonics M2, S2, N2, K1 and O1 these are plotted in the upper two panels of Figure 12 to 16. The lower two panels show the situation before and after assimilating these observations into the tide model.

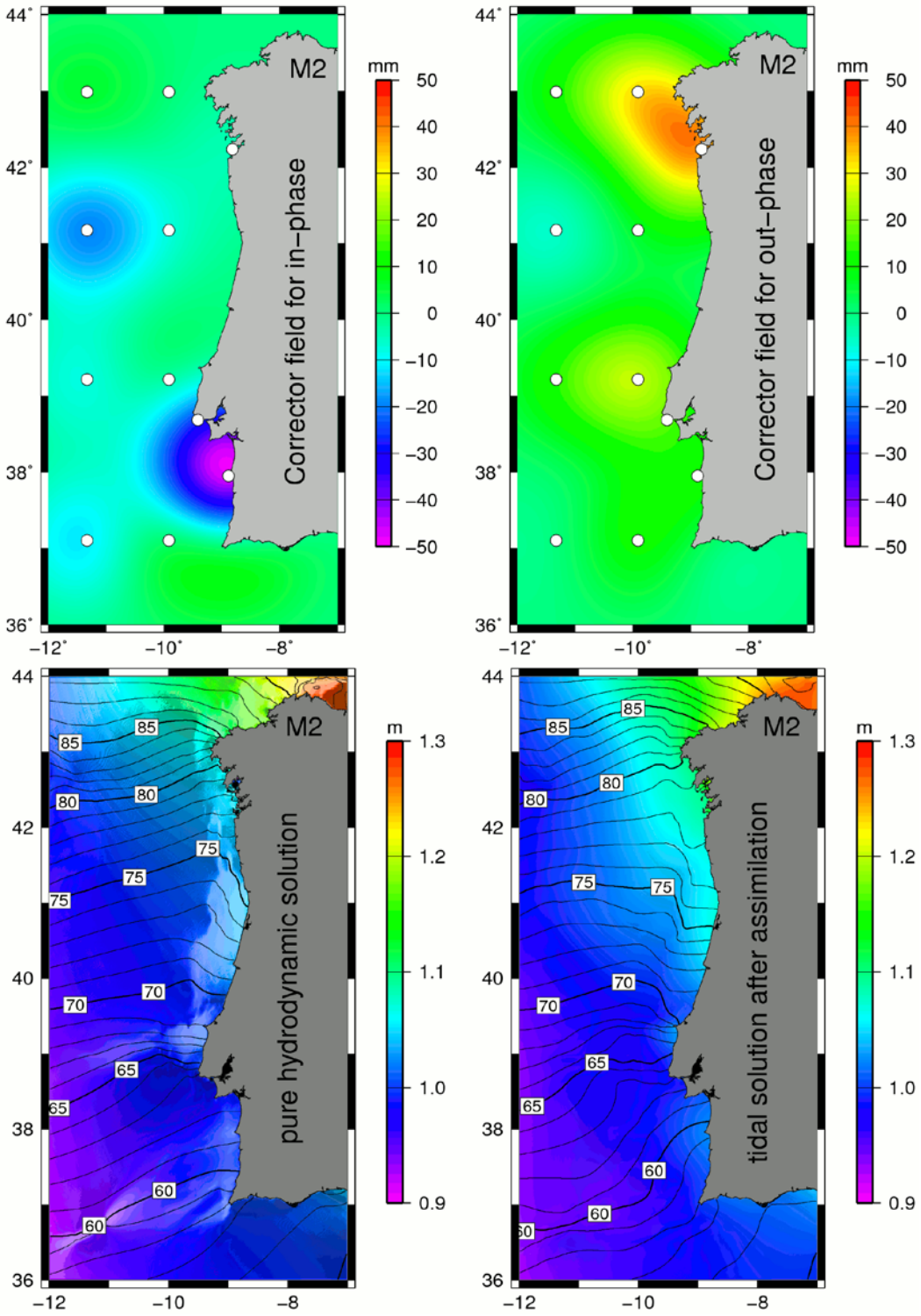

Fig. 12. The corrector fields for harmonic M2 and their effect on the tidal solution.

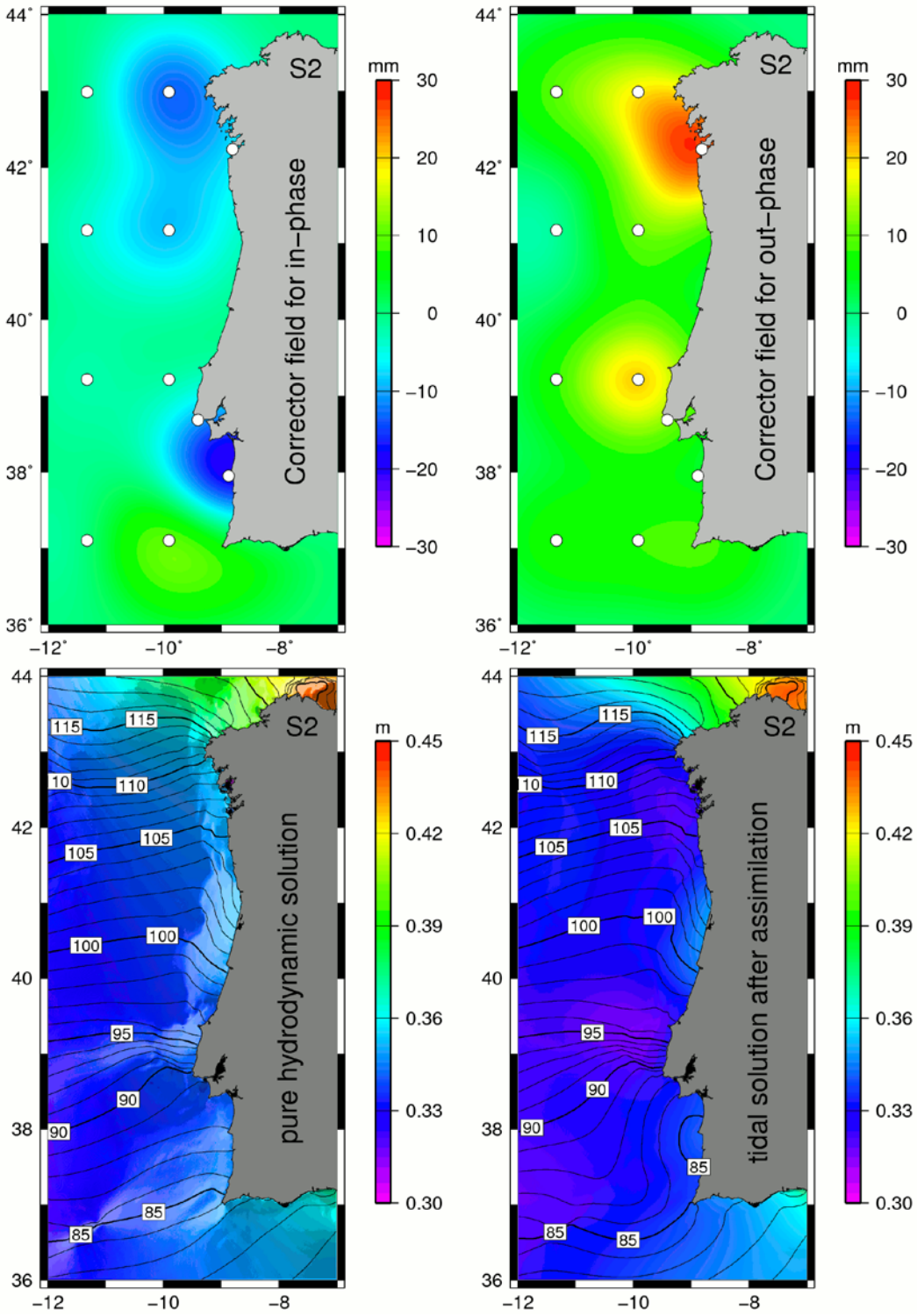

Fig. 13. The corrector fields for harmonic S2 and their effect on the tidal solution.

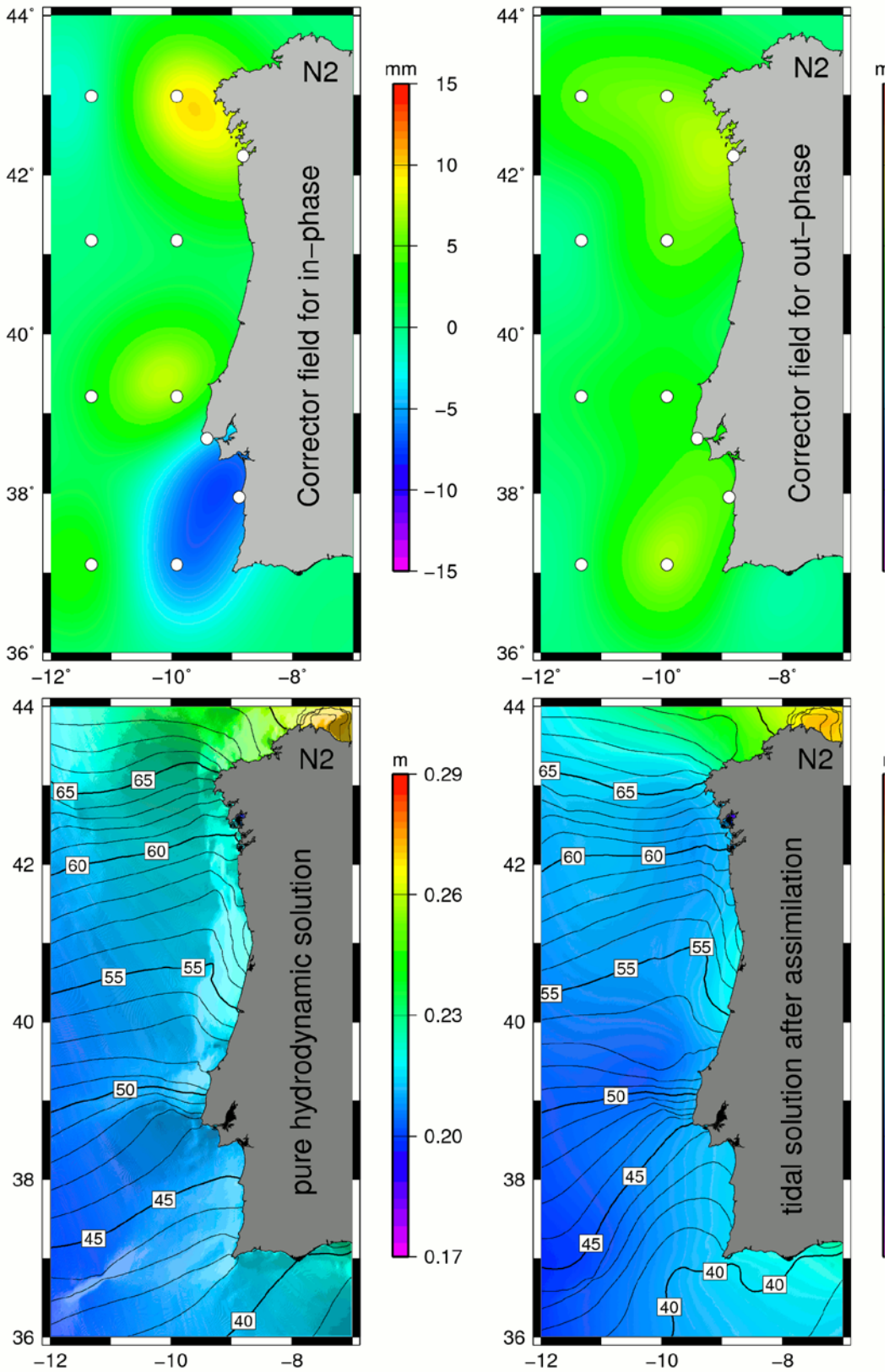

Fig. 14. The corrector fields for harmonic N2 and their effect on the tidal solution.

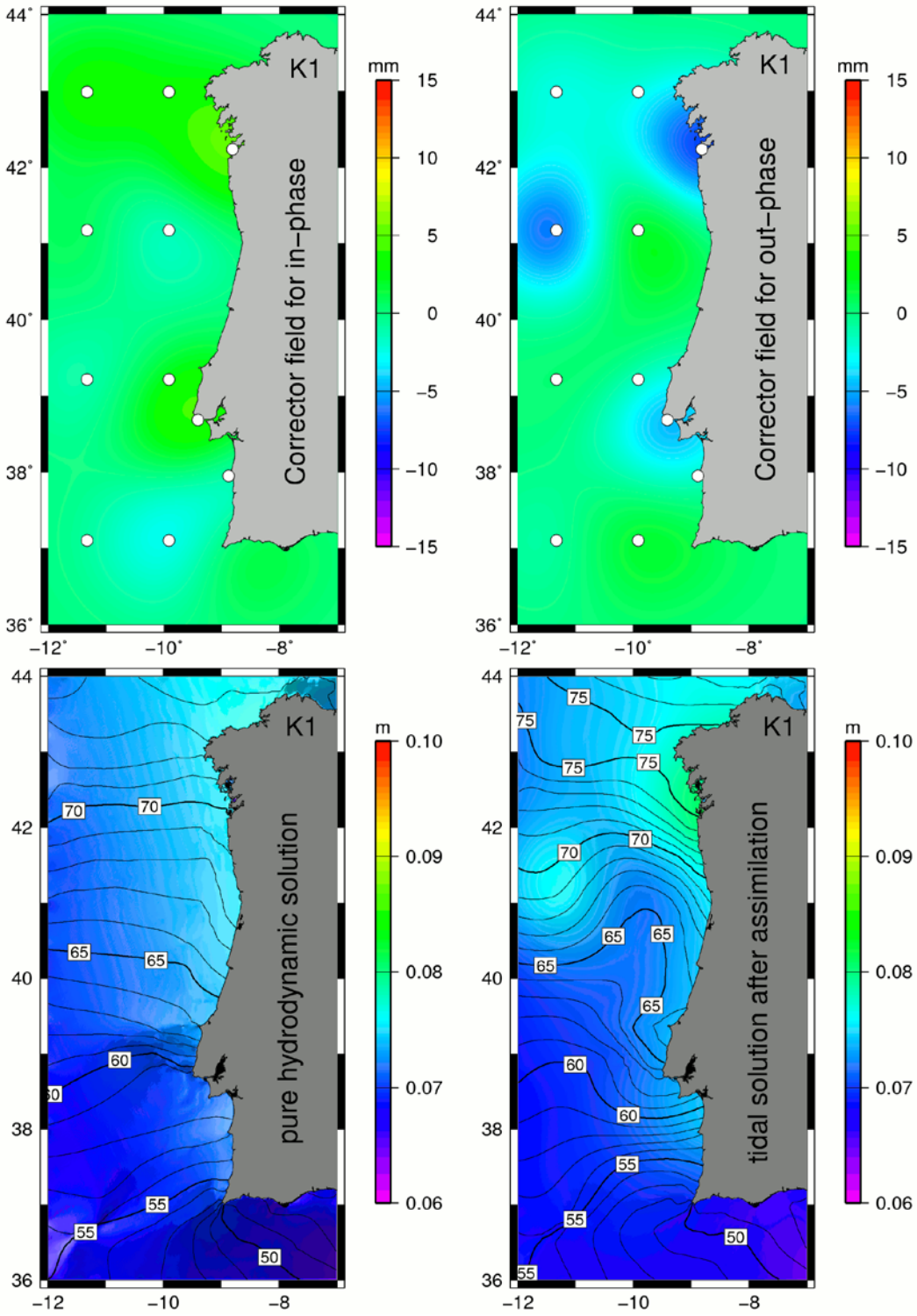

Fig. 15. The corrector fields for harmonic K1 and their effect on the tidal solution.

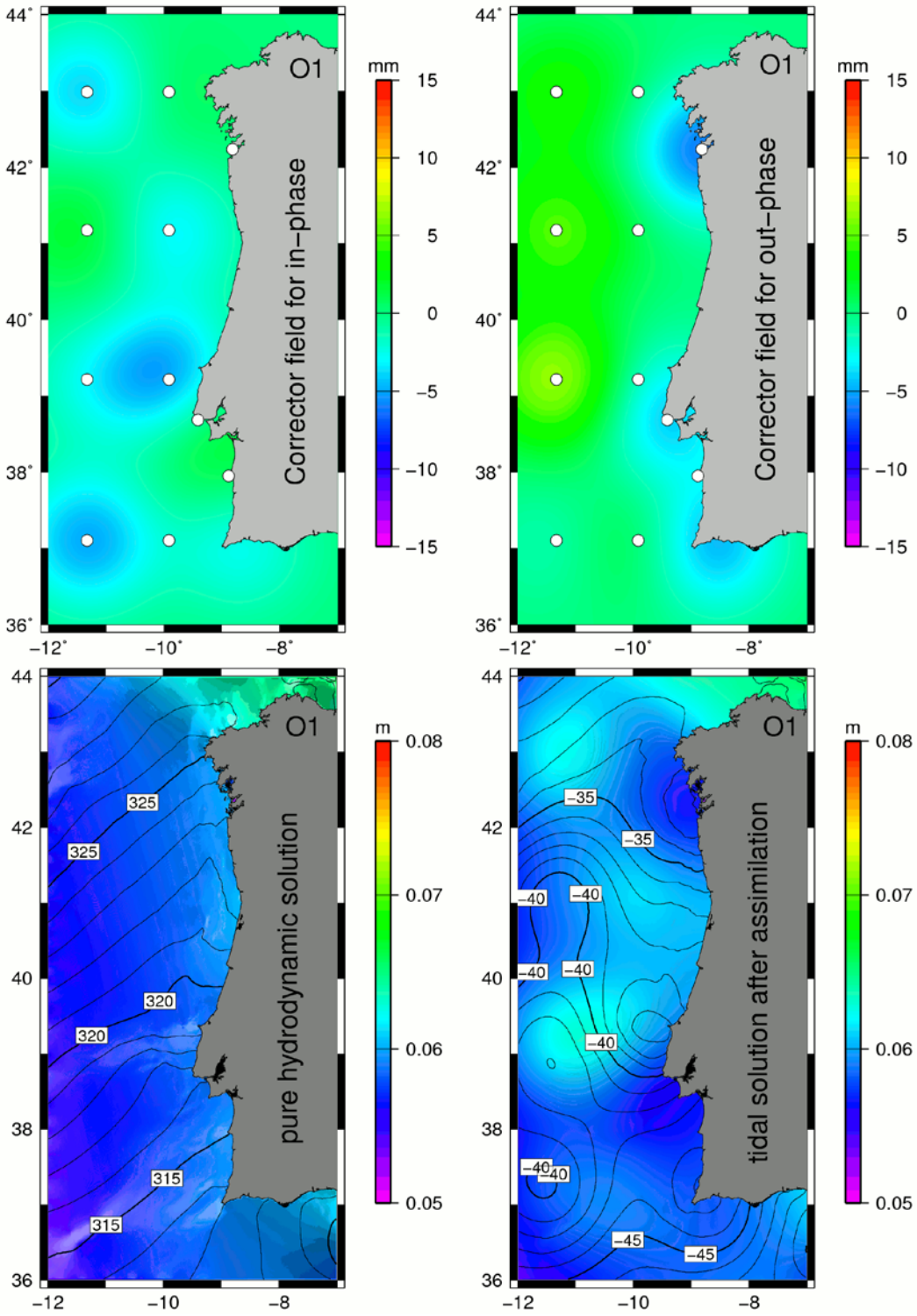

Fig. 16. The corrector fields for harmonic O1 and their effect on the tidal solution.

5. Transformation of the tidal maps into tidal elevations

The tidal maps have been converted into maps of tidal elevation using the hardisp program of Duncan Agnew which will be part of the IERS technical conventions (IERS, 2003). Instead of using only a few harmonics, normally less than 40, this program uses more than 150 harmonics of the complete tidal potential. The amplitude and phase-lags of the other smaller harmonics, which have not been discussed in this report, are obtained by fitting a polynomial through the 4 main semi-diurnal harmonics, or through the 4 main diurnal harmonics. Because the response of the ocean tides in front of the West Iberian Margin are reasonably smooth, this is a suitable method for use in this region.

To verify that our program works correctly, we have compared our computed tidal elevations with those observed at the Leixões tide gauge for the first 5 days of January 1991, see Figure 17. In this figure one can see the observed sea-level in red and the residual sea-level after subtracting our predicted tidal elevations. The tidal signal is clearly eliminated.

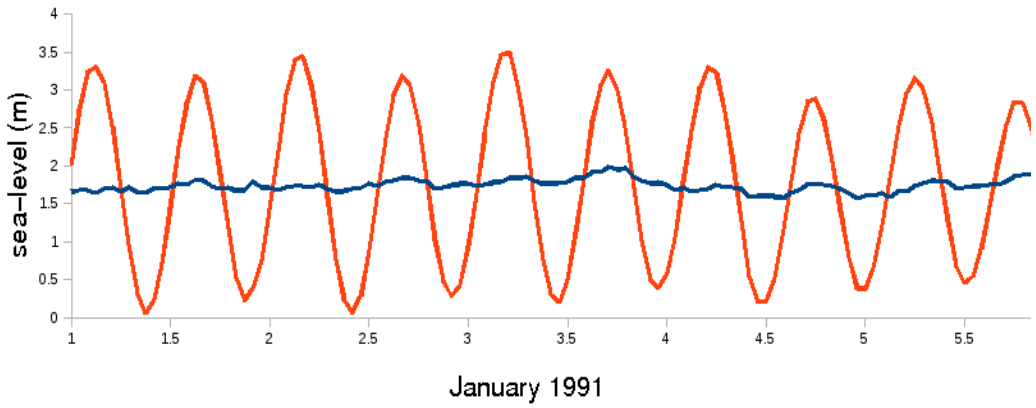

Fig. 17. The observed sea-level at Leixões in red and the sea-level after subtracting the predicted tides using the WITM tidal maps.

Note that in a harbour there are mostly non-linear effects which limit the applicability of our assumption of a smooth variation of the response of the ocean over several tidal frequencies. Nevertheless, our approach seems to produce good results even in this difficult environment.

The computed tides have an uncertainty of around 1 cm. This is mostly due to uncertainties in the forcing at the open boundaries and especially due to uncertainty in the bottom friction model and its parameters. Furthermore, there are relatively few observations in this region to constrain the tide model. If there were more observations then the lack of a good physical model for the tides could be solved by forcing the solutions to fit the real observed tides. For the margin in front of the West Iberian coast this is not possible. As a result, no attempt has been made to compute the non-linear tides such as M4. At Cascais the amplitude of this harmonic reaches 1 cm and is thus just within the noise level. In the open ocean the amplitude is even less.

We have also computed tidal solutions using the ETOPO2 bathymetry to investigate its influence. We could not detect a significant influence, the bottom friction modelling is much more important, and no efforts were made to improve the ETOPO1 bathymetry.

Finally, an example of a tidal elevation map for 0:00am on 1 January 1991 is given in Figure 18.

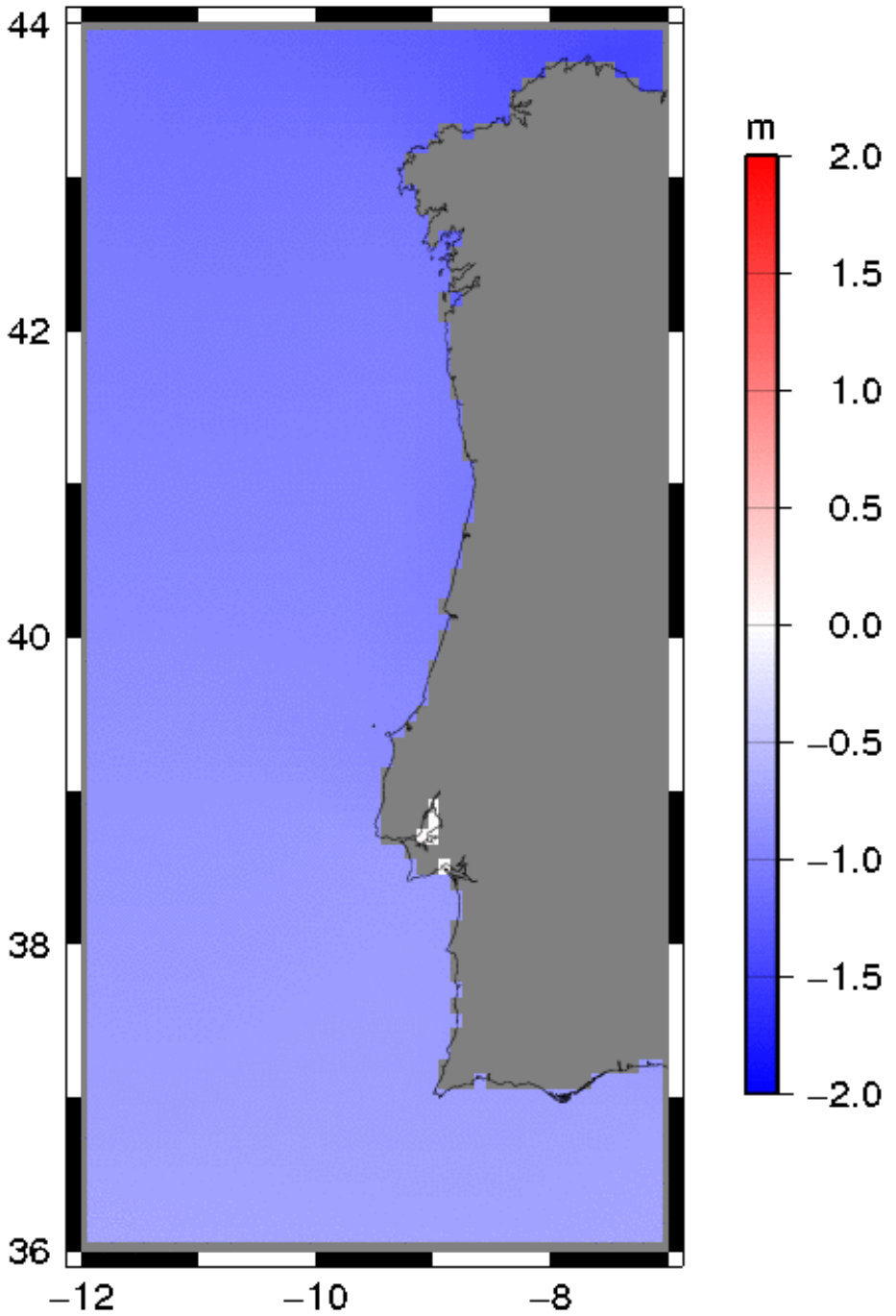

Fig 18. The computed tidal elevations at 0:00am, 1 January 1991.

6. Conclusions

A local tide model, WITM (West Iberian Tide Model) has been computed for the region 12ºW ≤ λ ≤ 7ºW and l36ºN ≤ φ ≤ 44ºN, for the period 1991-2005. The model includes the main tidal harmonics M2, S2, N2, K2, K1, O1, P1, Q1, Mf, Mm and Ssa.

This model has been computed with a time sampling of 30 minutes and a spatial sampling of 0.01°x0.01°.

To validate our model results with have performed tidal analyses on residual satellite altimetry time-series for the TOPEX/Poseidon, Jason 1& 2 and Envisat satellite at cross-over points. The results for the Envisat satellite are too noisy and were not used in this study.

In addition, we have also collected from the literature the tidal harmonics for tide gauges that are available in our area of research. Comparison with tide gauge data and the tidal harmonics derived from satellite altimetry data show that our model performs well in comparison with recent global ocean tide models which have these observations assimilated into them.

An exception is the comparison of our tide model with the tide gauge observations at Leixões. The exact reasons for this misfit are not known. This may be due to local effects around Leixões or bad bathymetry in our model.

This problem could be solved if better bathymetry from the Hydrographic Institute were available for this study, which unfortunately was not possible to obtain.

After the tidal maps for the main harmonics were computed, the results were smoothly adjusted to fit the TP observations at the cross-over points perfectly.

Finally, the tidal maps were converted into maps of tidal elevations using the hardisp program.

References

Amante, C. and B. W. Eakins (2009), ETOPO1 1 Arc-Minute Global Relief Model: Procedures, Data Sources and Analysis. NOAA Technical Memorandum NESDIS NGDC-24, 19 pp, March 2009.

Benavent, M., Arnoso, J., and Montesinos, F. G. (2009). Regional ocean tide loading modelling around the Iberian Peninsula. Journal of Geodynamics, 48:132–137.

Egbert, G. D., Bennett, A. F., and Foreman, M. G. G. (1994). TOPEX/POSEIDON tides estimated using a global inverse model. J. Geophys. Res., 99(C12):24,821–24,852.

Egbert, G.D., and S.Y. Erofeeva, (2002): Efficient inverse modelling of barotropic ocean tides, J. Atmos. Oceanic Technol., 19(2), 183-204.

Fanjul, E. (1997). A description of the tides in the Eastern North Atlantic. Progress in Oceanography, 40:217–244.

Foreman,M. G. G., Cherniawsky, J. Y., and Ballantyne, V. A. (2009). Versatile Harmonic Tidal Analysis: Improvements and Applications. Journal of Atmospheric and Oceanic Technology, 26:806–817.

Fortunato, A. (2002). Tidally generated shelf waves off the western Iberian coast. Continental Shelf Research, 22:1935–1950.

IERS Conventions (2003). Dennis D. McCarthy and Gérard Petit. (IERS Technical Note ; 32) Frankfurt am Main: Verlag des Bundesamts für Kartographie und Geodäsie, 2004. 127 pp., paperback, ISBN 3-89888-884-3 (print version)

Jayne, S.R. and St. Laurent, L.C. (2001), Parameterizing Tidal Dissipation over Rough Topography, Geophysical Research Letters, 28(5), 811-814.

Lee, J.C, Kim, C.S., and Jung, K.T. (2001), Comparison of Bottom Friction Formulations for Single-Constituents Tidal Simulations in Kyunggi Bay, Estuarine, Coastal and Shelf Science, 53, 701-715.

Lyard, F., F. Lefevre, T. Letellier, O. Francis, (2006), Modelling the global ocean tides: insights from FES2004, Ocean Dynamics, 56, 394-415.

Marta-Almeida, M. and Dubert, J. (2006). The structure of tides in the Western Iberian region. Continental Shelf Research, 26:385–400.

Matsumoto, K., T. Takanezawa, and M. Ooe (2000), Ocean Tide Models Developed by Assimilating TOPEX/POSEIDON Altimeter Data into Hydrodynamical Model: A Global Model and a Regional Model Around Japan, Journal of Oceanography, 56, 567-581.

Ray, R. D. (1999), A Global Ocean Tide Model From TOPEX/POSEIDON Altimetry: GOT99.2. NASA Technical Memorandum 209478.

Sauvaget, P., David, E., and Soares, C. G. (2000). Modelling tidal currents on the coast of Portugal. Coastal Engineering, 40(4):393–409.

Savcenko R., Bosch W. (2008), EOT08a − empirical ocean tide model from multi-mission satellite altimetry. DGFI Report No. 81, Deutsches Geodätisches Forschungsinstitut (DGFI), München.

Schwiderski, E. W. (1980). On charting global ocean tides. Rev. Geophys. Space Phys., 18(1):243–268.

Smithson M.J. (1992), IAPSO scientific publication # 35.

Appendix A

This appendix contains the tidal maps for the 11 main harmonics.

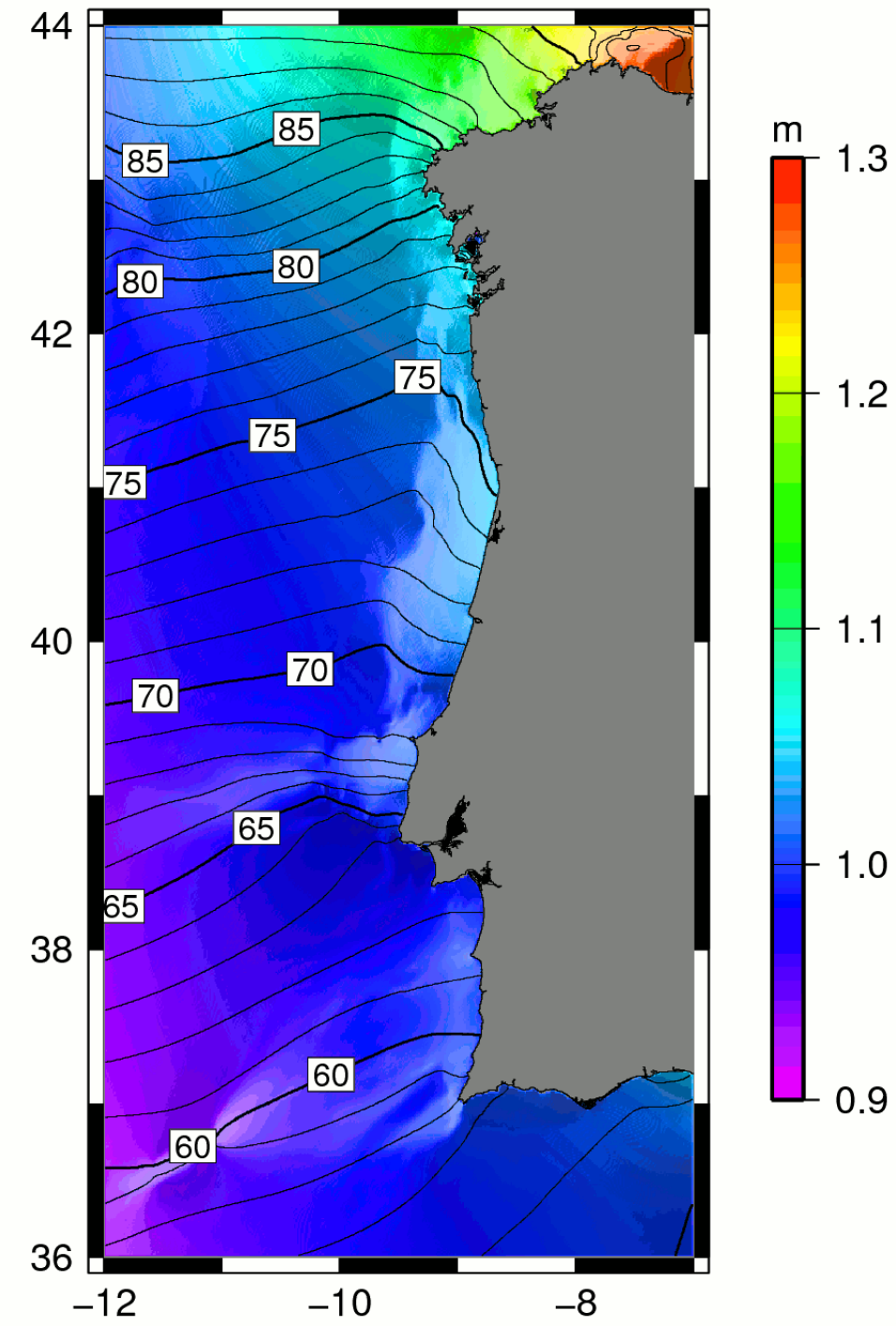

Fig 19. The computed tidal elevations for harmonic M2.

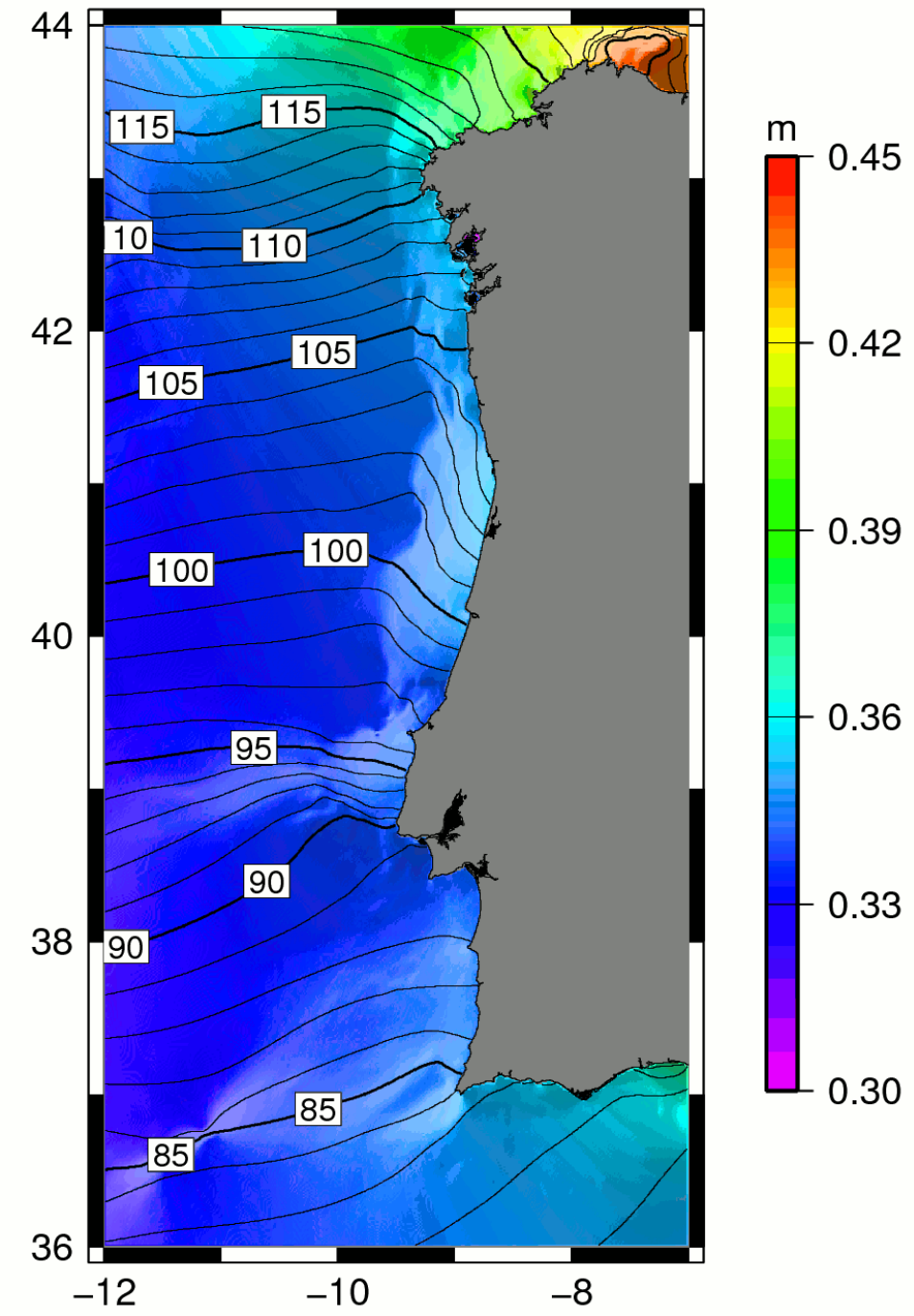

Fig 20. The same as for Fig. 19 but for harmonic S2

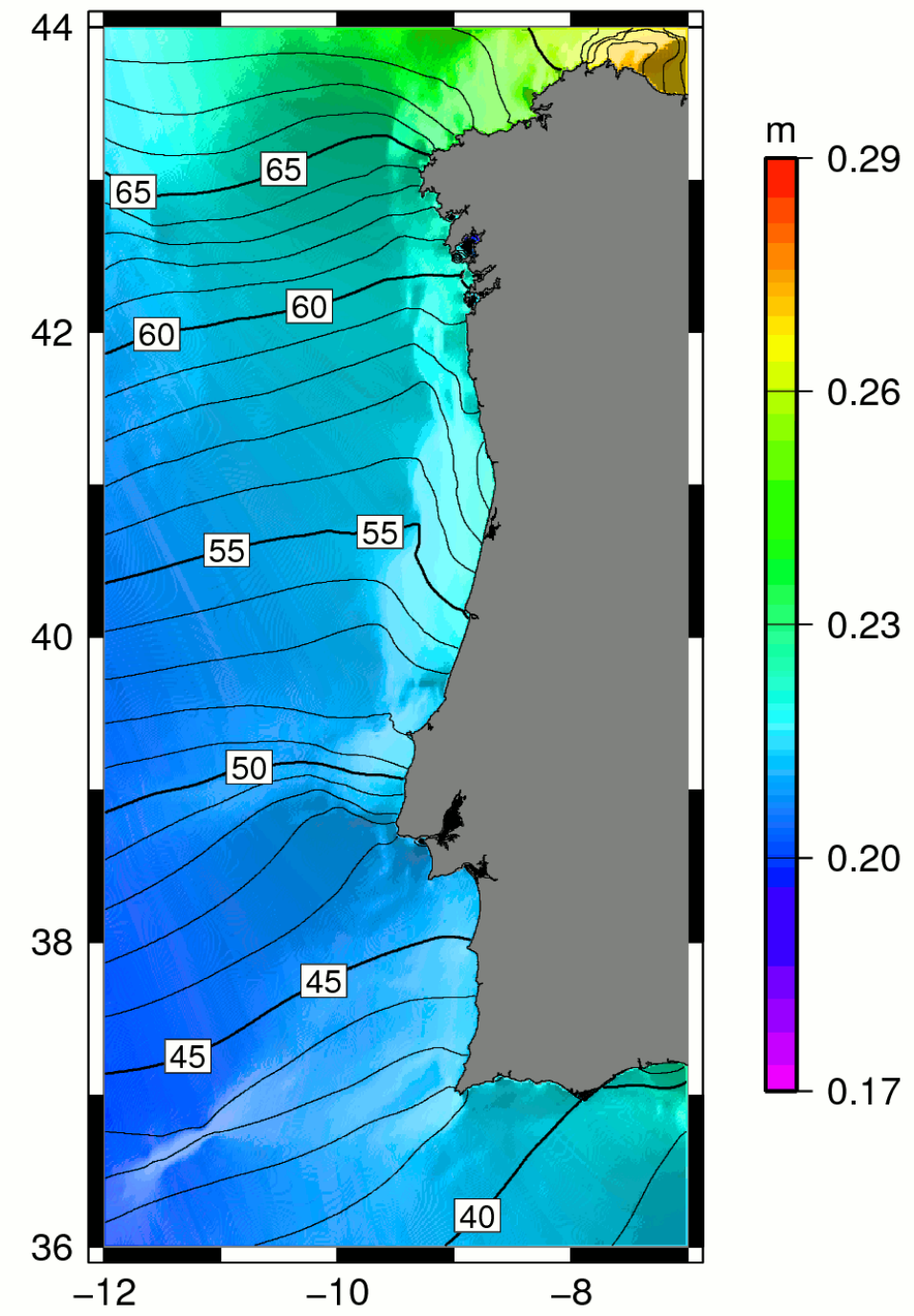

Fig 21. The same as for Fig. 19 but for harmonic N2.

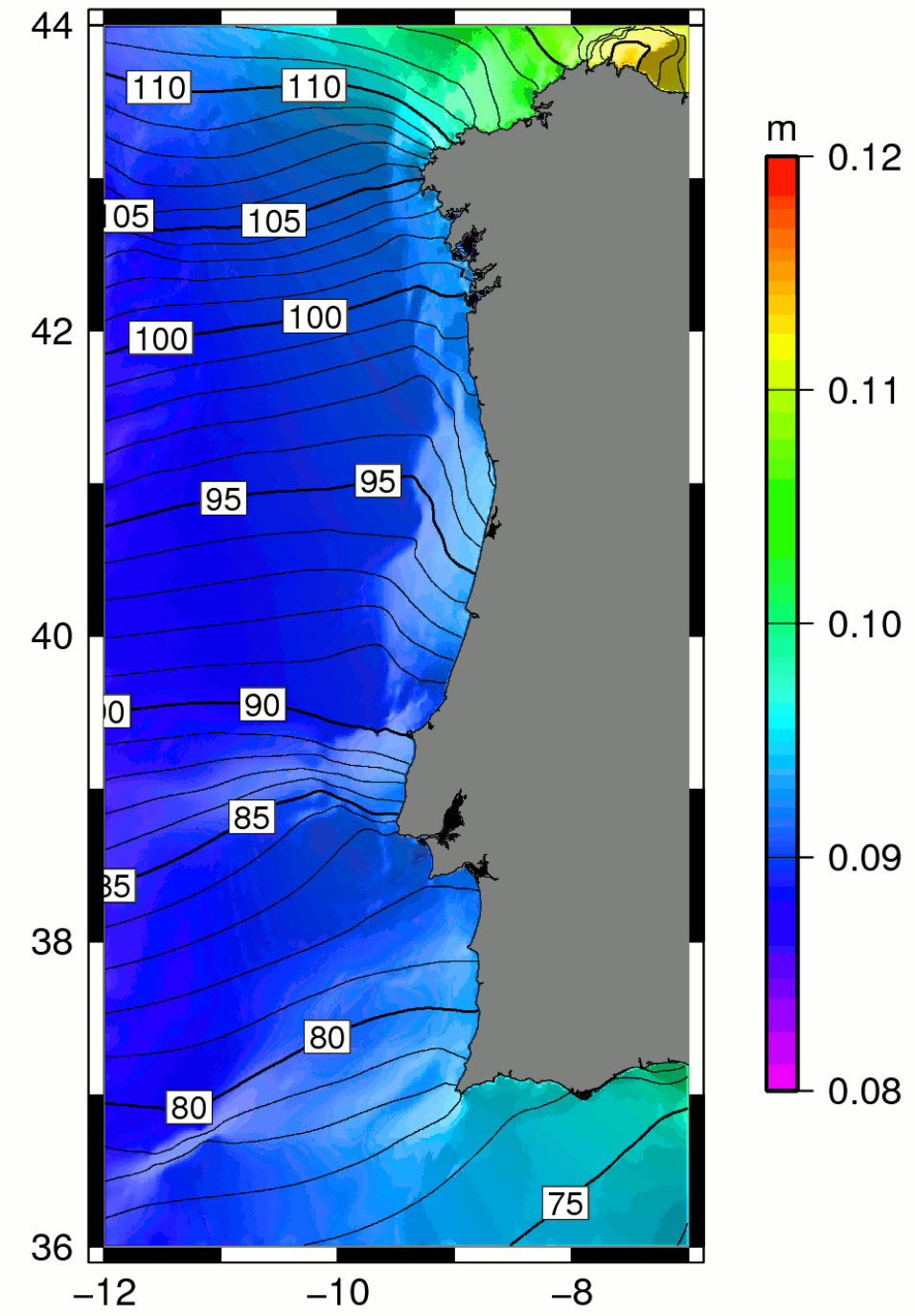

Fig 22. The same as for Fig. 19 but for harmonic K2.

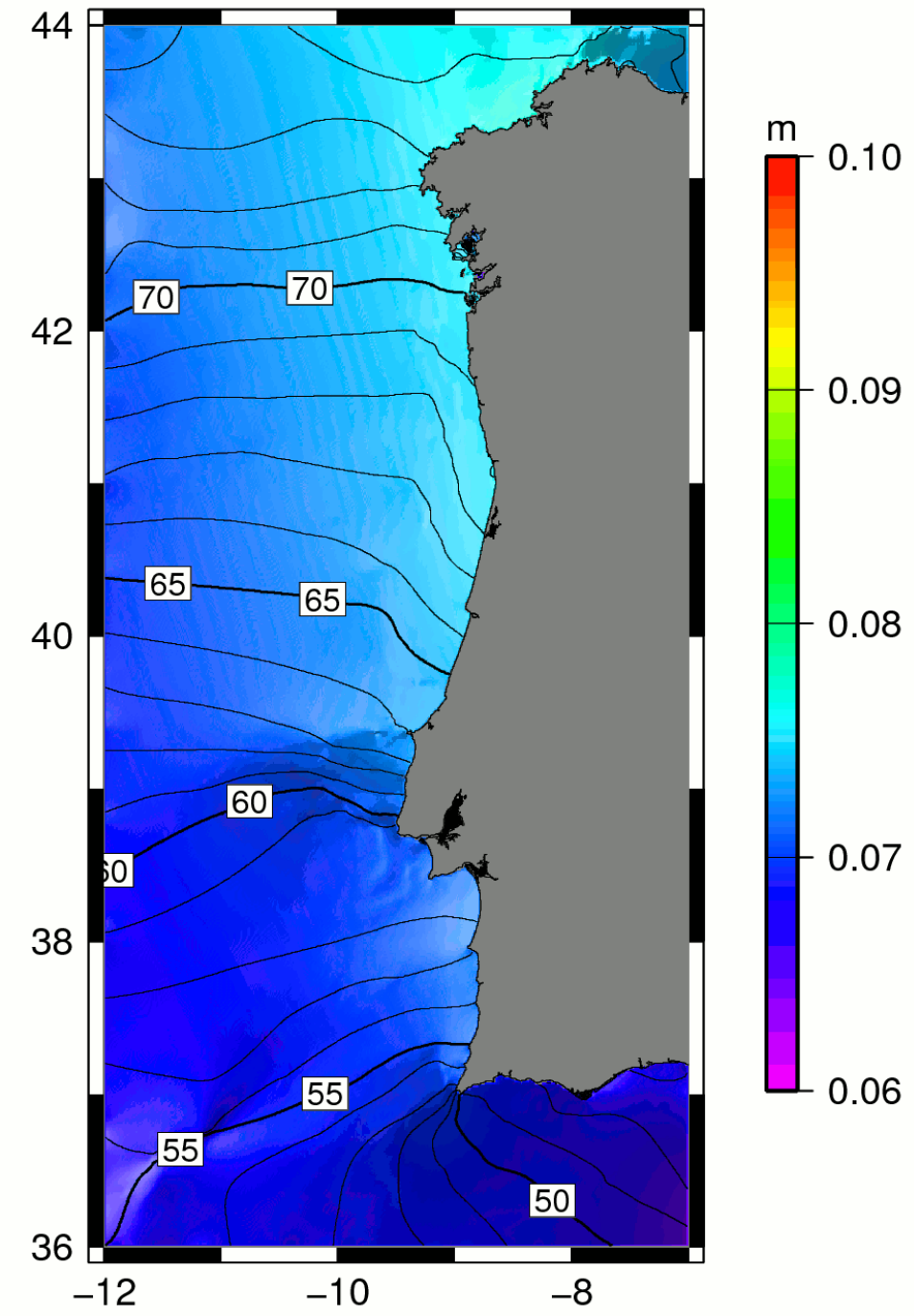

Fig. 23. The same as for Fig. 19 but for harmonic K1.

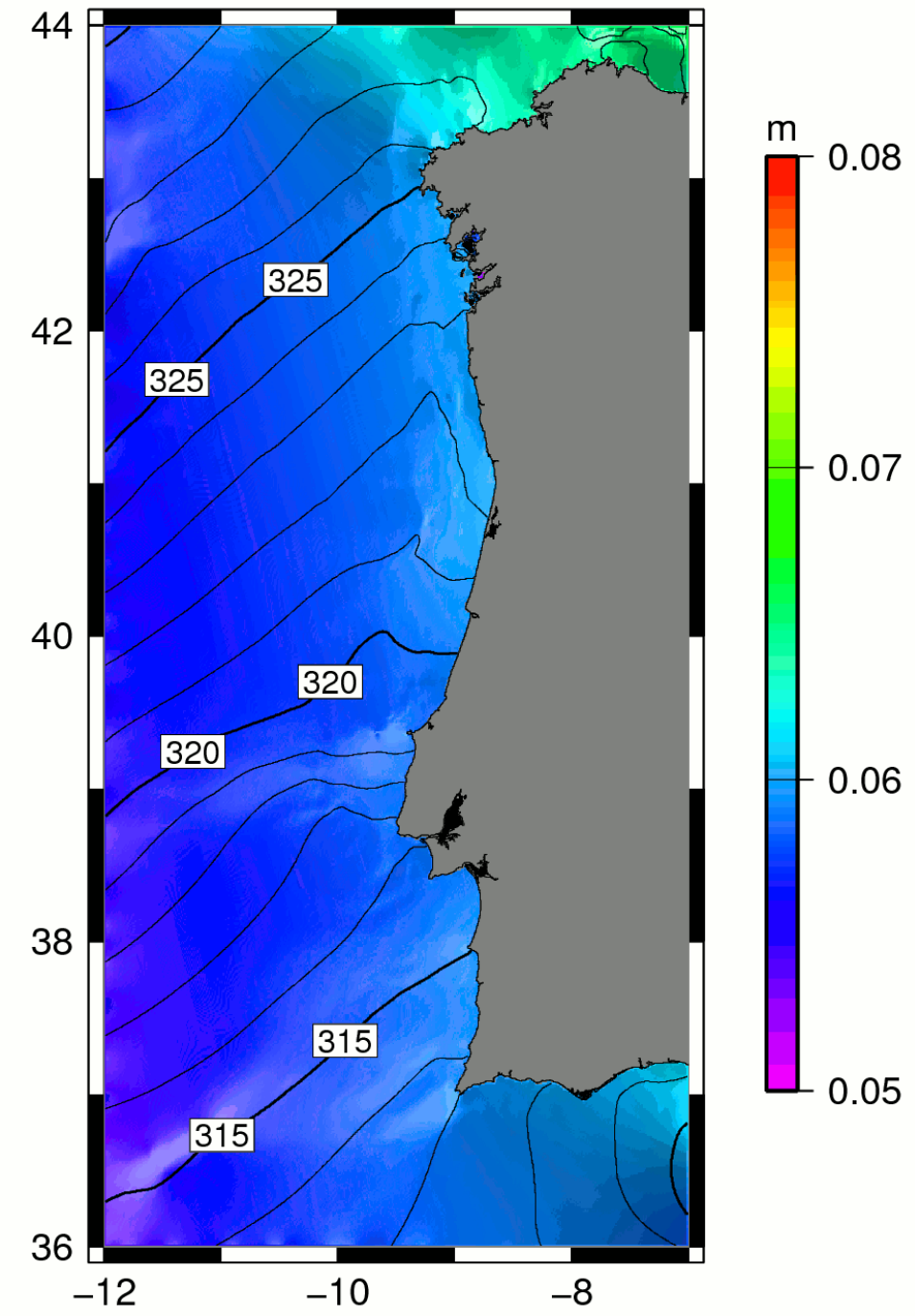

Fig. 24. The same as for Fig. 19 but for harmonic O1.

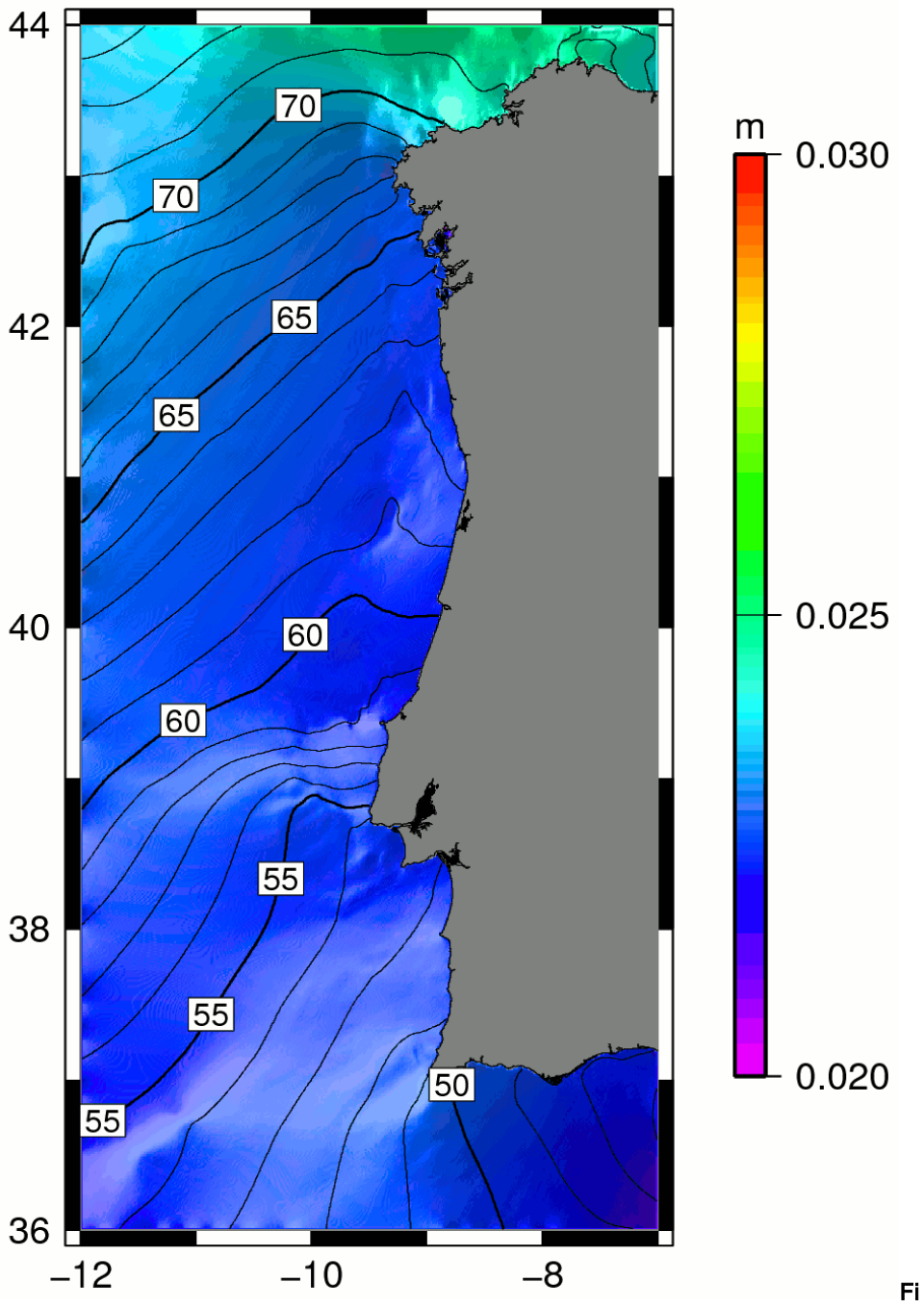

Fi

g 25. The same as for Fig. 19 but for harmonic P1.

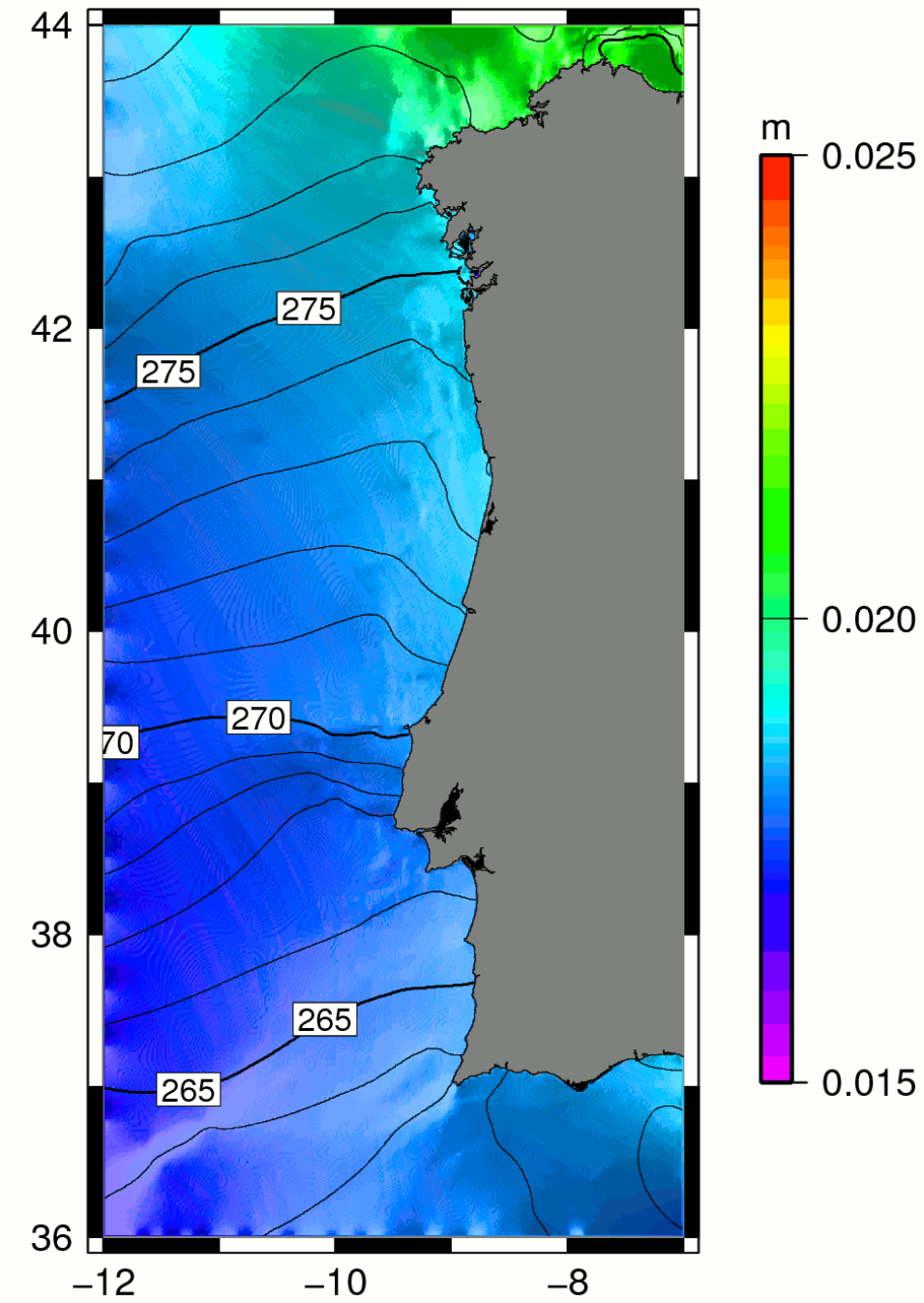

Fig. 26. The same as for Fig. 19 but for harmonic Q1.

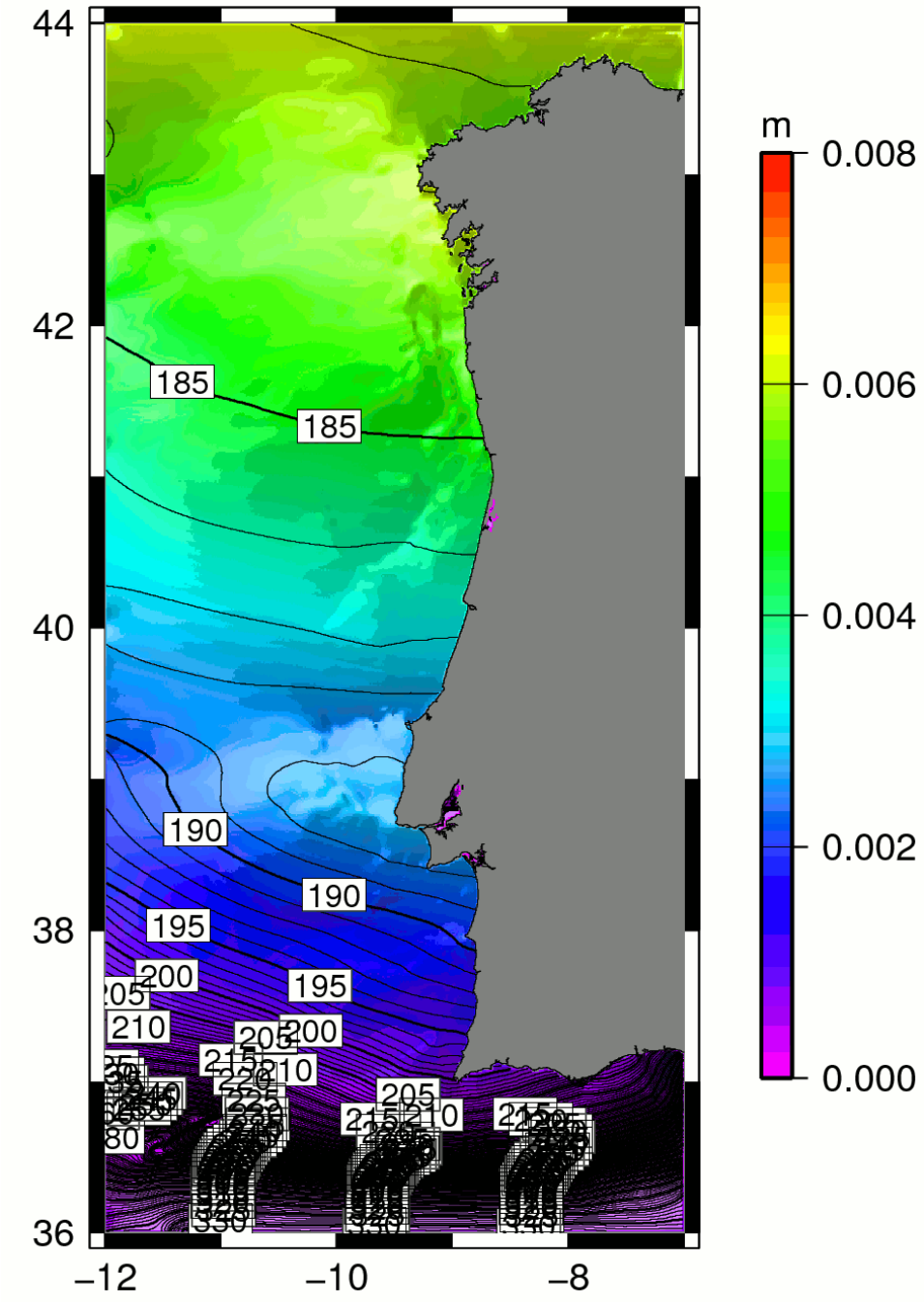

Fig. 27. The same as for Fig. 19 but for harmonic Mf.

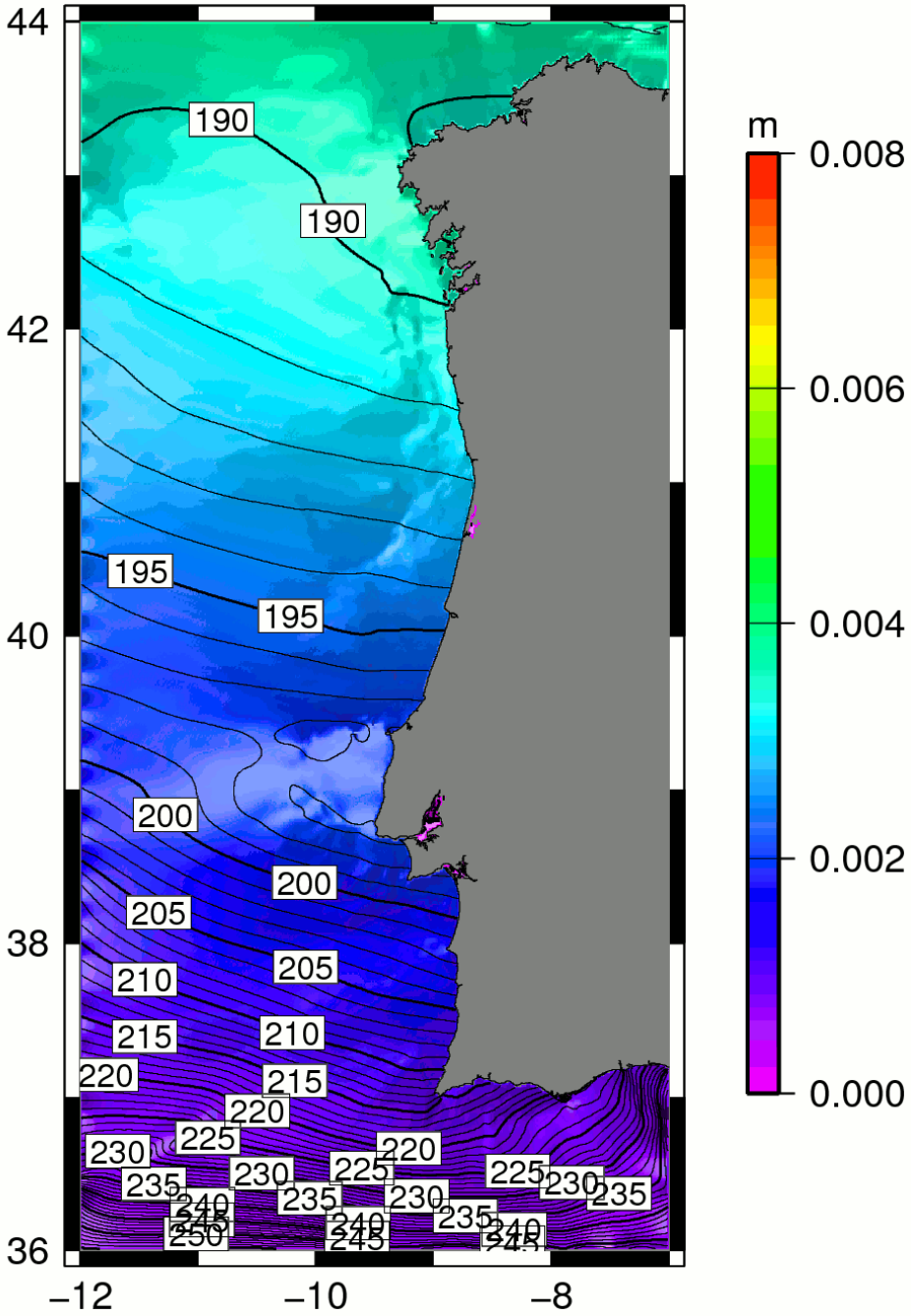

Fig. 28. The same as for Fig. 19 but for harmonic Mm.

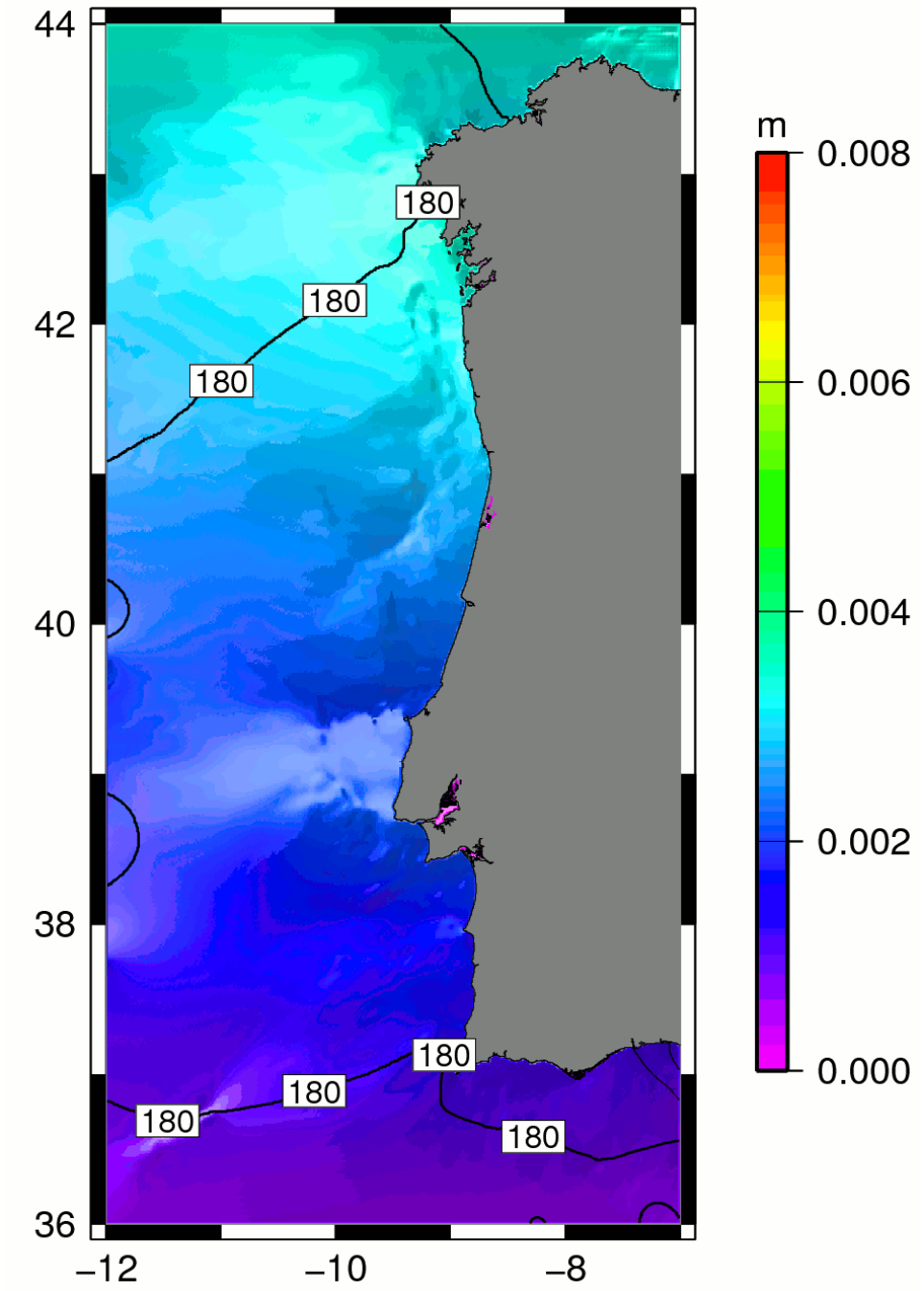

Fig. 29. The same as for Fig. 19 but for harmonic Ssa.

Appendix B

This section contains the comparison results between TP cross-over points and tide gauges.

Table 1: The observed tide values for harmonic M2 at the cross-over points of the TP satellite and the values provided by the tide models.

	Gauge	FES2004	TPXO.7.2	GOT4.7	IBER01	WITM
Location	mm(degrees)	mm(degrees)	mm(degrees)	mm(degrees)	mm(degrees)	mm(degrees)
crossover 0	890(54)	899(54)	895(54)	892(55)	890(54)	
crossover 1	1280(94)	1283(94)	1274(93)	1281(93)	1260(92)	
crossover 2	969(54)	965(54)	959(54)	958(54)	959(54)	
crossover 3	1043(91)	1046(91)	1049(91)	1042(91)	1029(90)	
crossover 4	997(54)	995(54)	993(54)	990(55)	989(54)	
crossover 5	1084(83)	1087(83)	1078(83)	1082(83)	1068(82)	1051(83)
crossover 6	1192(92)	1191(92)	1186(92)	1189(92)	1169(91)	
crossover 7	924(69)	924(69)	916(69)	916(69)	915(69)	
crossover 8	969(76)	985(75)	978(76)	977(76)	969(76)	979(75)
crossover 9	936(62)	943(61)	935(61)	935(61)	932(61)	941(61)
crossover 10	1010(69)	1013(68)	1005(68)	998(68)	1004(68)	988(68)
crossover 11	956(83)	963(84)	952(83)	958(84)	943(83)	
crossover 12	986(54)	985(54)	981(54)	979(54)	984(54)	
crossover 13	1031(84)	1025(84)	1015(84)	1020(84)	1004(84)	1019(84)
crossover 14	1123(91)	1117(91)	1119(91)	1113(91)	1090(90)	
crossover 15	924(76)	940(76)	930(76)	933(76)	928(76)	
crossover 16	1009(74)	1026(75)	1020(75)	1017(75)	1007(75)	1005(74)
crossover 17	903(62)	911(62)	904(62)	903(62)	899(62)	
crossover 18	1259(93)	1247(93)	1239(93)	1245(93)	1222(92)	
crossover 19	925(55)	936(54)	930(54)	929(55)	919(54)	
crossover 20	981(60)	977(60)	967(60)	968(60)	960(60)	972(60)
crossover 21	965(91)	980(91)	978(91)	976(91)	958(90)	
crossover 22	970(69)	966(68)	961(68)	956(69)	951(68)	961(68)

Table 2: The same as for Table 1 but at the tide gauges.

	Gauge	FES2004	TPXO.7.2	GOT4.7	IBER01	WITM
Location	mm(degrees)	mm(degrees)	mm(degrees)	mm(degrees)	mm(degrees)	mm(degrees)
RM1 / IAPSO-1.1.43	789(55)	946(60)	939(59)	939(60)	938(59)	951(59)
RD4 / IAPSO-1.1.44	1045(59)	982(59)	971(59)	972(59)	964(59)	978(59)
LEIXOES	1032(73)	1055(75)	1067(73)	1042(74)	1032(73)	1040(75)
CASCAIS (CASC)	991(64)	1004(64)	979(65)	980(64)	997(64)	988(63)
SINES	983(64)	999(62)	974(62)	988(63)	976(63)	995(61)
LAGOS	1006(57)	1008(57)	998(57)	997(58)	1008(58)	1005(57)
VIGO	1086(78)	1137(80)	1100(77)	1122(81)	1098(76)	1049(77)

Table 3: The vector differences between the tidal values at the cross-over points and the values provided by the tide models for harmonic M2.

	FES2004	TPXO.7.2	GOT4.7	IBER01	WITM
Location	mm(degrees)	mm(degrees)	mm(degrees)	mm(degrees)	mm(degrees)
crossover 0	10(1)	6(1)	10(1)	3(0)	
crossover 1	3(0)	12(1)	4(0)	42(3)	
crossover 2	5(1)	11(1)	10(1)	11(1)	
crossover 3	5(0)	6(1)	1(0)	18(2)	
crossover 4	2(0)	4(0)	11(1)	8(1)	
crossover 5	4(0)	7(1)	2(0)	18(2)	33(3)
crossover 6	6(0)	6(1)	4(0)	31(3)	
crossover 7	3(0)	8(1)	8(1)	9(1)	
crossover 8	19(2)	10(1)	11(1)	5(1)	20(2)
crossover 9	13(1)	13(1)	7(1)	9(1)	11(1)
crossover 10	7(1)	7(1)	17(2)	10(1)	25(3)
crossover 11	10(1)	5(0)	7(1)	15(2)	
crossover 12	2(0)	5(1)	11(1)	3(0)	
crossover 13	8(1)	16(2)	14(1)	29(3)	13(1)
crossover 14	7(1)	4(0)	10(1)	39(3)	
crossover 15	17(2)	6(1)	9(1)	5(1)	
crossover 16	18(2)	16(2)	10(1)	9(1)	10(1)
crossover 17	8(1)	2(0)	5(1)	4(0)	
crossover 18	14(1)	20(2)	15(1)	44(4)	
crossover 19	12(1)	9(1)	4(0)	10(1)	
crossover 20	4(0)	14(1)	14(1)	21(2)	10(1)
crossover 21	15(2)	14(1)	11(1)	18(2)	
crossover 22	9(1)	12(1)	15(2)	20(2)	15(2)

Table 4: The same as Table 3 but at the tide gauges.

	FES2004	TPXO.7.2	GOT4.7	IBER01	WITM
Location	mm(degrees)	mm(degrees)	mm(degrees)	mm(degrees)	mm(degrees)
RM1 / IAPSO-1.1.43	168(21)	161(20)	163(21)	160(20)	170(22)
RD4 / IAPSO-1.1.44	63(6)	74(7)	73(7)	81(8)	67(6)
LEIXOES	37(4)	36(4)	28(3)	2(0)	43(4)
CASCAIS (CASC)	20(2)	19(2)	16(2)	8(1)	31(3)
SINES	37(4)	38(4)	27(3)	24(2)	48(5)
LAGOS	2(0)	8(1)	16(2)	10(1)	3(0)
VIGO	61(6)	23(2)	69(6)	33(3)	39(4)